Co-culture of human induced pluripotent stem cell-derived retinal pigment epithelial cells and endothelial cells on double collagen-coated honeycomb films

Acta Biomaterialia 101 (2020) 327–343

Contents lists available at ScienceDirect

Acta Biomaterialia

journal homepage: www.elsevier.com/locate/actbio

Full length article

Co-culture of human induced pluripotent stem cell-derived retinal pigment epithelial cells and endothelial cells on double collagen-coated honeycomb films

Maria Teresa Calejo[a,*], Jaakko Saari[a], Hanna Vuorenpää[a], Elina Vuorimaa-Laukkanen[b], Pasi Kallio[a], Katriina Aalto-Setälä[a,c], Susanna Miettinen[a,d], Heli Skottman[a], Minna Kellomäki[a], Kati Juuti-Uusitalo[a,*]

[a] Faculty of Medicine and Health Technology, Tampere University, Tampere, Finland
[b] Faculty of Engineering and Natural Sciences, Tampere University, Tampere, Finland
[c] Heart Hospital, Tampere University Hospital, Tampere, Finland
[d] Research, Development and Innovation Centre, Tampere University Hospital, Tampere, Finland

ARTICLE INFO

Article history:
Received 9 August 2019
Revised 25 October 2019
Accepted 1 November 2019
Available online 8 November 2019

Keywords:
Polylactide
Breath figures
Co-culture
hiPSC-endothelial cells
hiPSC-RPE

ABSTRACT

In vitro cell culture models representing the physiological and pathological features of the outer retina are urgently needed. Artificial tissue replacements for patients suffering from degenerative retinal diseases are similarly in great demand. Here, we developed a co-culture system based solely on the use of human induced pluripotent stem cell (hiPSC)-derived cells. For the first time, hiPSC-derived retinal pigment epithelium (RPE) and endothelial cells (EC) were cultured on opposite sides of porous polylactide substrates prepared by breath figures (BF), where both surfaces had been collagen-coated by Langmuir–Schaefer (LS) technology. Small modifications of casting conditions during material preparation allowed the production of free-standing materials with distinct porosity, wettability and ion diffusion capacity. Complete pore coverage was achieved by the collagen coating procedure, resulting in a detectable nanoscale topography. Primary retinal endothelial cells (ACBRI181) and umbilical cord vein endothelial cells (hUVEC) were utilised as EC references. Mono-cultures of all ECs were prepared for comparison. All tested materials supported cell attachment and growth. In mono-culture, properties of the materials had a major effect on the growth of all ECs. In co-culture, the presence of hiPSC-RPE affected the primary ECs more significantly than hiPSC-EC. In consistency, hiPSC-RPE were also less affected by hiPSC-EC than by the primary ECs. Finally, our results show that the modulation of the porosity of the materials can promote or prevent EC migration.

In short, we showed that the behaviour of the cells is highly dependent on the three main variables of the study: the presence of a second cell type in co-culture, the source of endothelial cells and the biomaterial properties. The combination of BF and LS methodologies is a powerful strategy to develop thin but stable materials enabling cell growth and modulation of cell-cell contact.

Statement of significance

Artificial blood-retinal barriers (BRB), mimicking the interface at the back of the eye, are urgently needed as physiological and disease models, and for tissue transplantation targeting patients suffering from degenerative retinal diseases. Here, we developed a new co-culture model based on thin, biodegradable porous films, coated on both sides with collagen, one of the main components of the natural BRB, and cultivated endothelial and retinal pigment epithelial cells on opposite sides of the films, forming a three-layer structure. Importantly, our hiPSC-EC and hiPSC-RPE co-culture model is the first to exclusively use human induced pluripotent stem cells as cell source, which have been widely regarded as an practical candidate for therapeutic applications in regenerative medicine.

* Corresponding authors.
E-mail address: teresa.rebelocalejo@tuni.fi (M.T. Calejo).

https://doi.org/10.1016/j.actbio.2019.11.002
1742-7061/

1. Introduction

Retinal degenerative diseases are estimated to affect millions of people worldwide, with numbers increasing every year due to the increased life expectancy and growth of the world population. Age-related macular degeneration (AMD) alone, a leading cause of irreversible blindness, is estimated to affect 30–50 million people globally [1]. Recent studies suggest a differential role of the choriocapillaris in AMD, where breakdown of the choroidal vasculature precedes the progressive degeneration of the thin retinal pigment epithelium (RPE) [2,3]. This thin monolayer of cells at the back of the eye is in direct contact with the photoreceptors and performs a number of essential roles for their survival and function. In the outer retina, the RPE is further sitting on the Bruch's membrane, a multilayer collagen- and elastin-rich extracellular matrix, that separates the RPE from the blood capillaries of the choroid [4]. As AMD progresses, these interfaces also become damaged, disrupting the retinal homoeostasis and leading to severe vision loss. In such cases, recovery of the lost vision may only be achieved by retinal transplantation, but the poor availability of allografts, together with the high risk of immune rejection, make this a rather limited solution [5].

Artificial tissue-engineered blood-retinal barriers (BRB), mimicking the RPE-choroid interface, hold high promise in cell replacement therapy for retinal regeneration. On the other hand, appropriate *in vitro* models of the BRB are urgently needed to understand the physiological and pathological aspects of the outer retina, especially in a time when awareness concerning the ethical aspects of *in vivo* animal studies is becoming globally spread [6]. In spite of the complexity of the BRB, most *in vitro* models so far are simple and use RPE mono-cultures to study RPE function and mechanisms of retinal diseases [6,7]. RPE mono-cultures are hardly representative of the complex physiology of the outer retina, where the interactions between RPE cells and choroidal endothelial cells (EC) are critical for the homoeostatic secretion of angiogenic and angiostatic factors [8]. *In vivo* studies have shown that interactions between RPE and ECs are critical for the survival of the choriocapillaris [9]; on the other hand, the up-regulated secretion of vascular endothelial growth factor (VEGF) by RPE is responsible by the pathogenesis of choroidal neovascularisation, which is one of the most important complications of impairing eye conditions such as AMD [10].

Examples of co-culture systems can be found in the literature, where RPE and EC have been cultured together as a cell mixture [11], or separated by commercial Transwell inserts [8,12–14], a hydrogel [15] or even an amniotic membrane [16]. The membranes that are typically used, however, are readily available materials, and little or no regard is given to the modulation of porosity and/or permeability across the material. In consistency, synthetic biodegradable polymer membranes have hardly been studied in co-culture of RPE and EC, in spite of the existence of multiple techniques allowing their easy preparation.

The breath figure (BF) method, in particular, is a simple, low-cost, solvent casting method to prepare porous films, characterised by a highly ordered hexagonal array of pores at the surface that resembles a honeycomb [17]. A key factor is the presence of high humidity conditions during film preparation, since the pores are created by the condensation of the water droplets onto the evaporating polymer solution. The evaporation of both the solvent and the water droplets leaves behind solid films with hexagonally packed pores, *i.e.* the so-called honeycomb films [17]. The method is also versatile, in that features such as pore size, pore shape, film thickness, permeability and surface wettability can be modulated by simply changing the variables of the process, such as polymer type and concentration, casting volume, solvent type and relative humidity [17,18]. In our previous work, we have successfully demonstrated the potential of biodegradable honeycomb films supporting the adhesion, growth and maturation of human stem cell-derived RPE (hESC-RPE) in mono-culture [19–21]. Recently, we have also described, for the first time, the deposition of a thin but contiguous layer of aligned collagen fibres onto the top surface of polylactide honeycomb films, using the Langmuir-Schaefer technique (LS). The Langmuir–Blodgett (LB)/LS technique is known as an elegant means for the fabrication of highly organised structures with molecular level precision, which can be transferred onto a solid substrate by vertical or horizontal deposition, respectively [22]. Even though the first studies on LB film deposition date back to the early 1930s [23], the literature is still extremely scarce in what concerns the use of the technique to prepare biomimetic biomaterials based on extracellular matrix components for tissue engineering applications. To the best of our knowledge, our study was the first where biodegradable polymer substrates were used for LS deposition, and as substrates for hESC-RPE [19]. The LS-coated honeycomb films demonstrated increased biocompatibility, due to the biomimetic properties of the collagen at the surface [19].

In this work, we took a step forward by exploring, for the first time, the potential of combining BF and LS technologies to prepare thin but free-standing, porous films, coated on both surfaces with a thin collagen-LS layer. High focus was given to the modulation of the porosity across the material, with the aim of producing thin biocompatible materials, capable of supporting the growth of RPE and EC cells in co-culture and preventing transmembrane cell migration, while allowing the flux of soluble factors secreted by the cells cultured on opposite sides of the material. The novelty of our work is further extended by the fact that it describes the first EC and RPE co-culture relying *solely* on human pluripotent stem cells (hPSC), specifically human induced-pluripotent stem cells (hiPSC) as cell source. In fact, *in vitro* retinal models typically use RPE and EC cells of primary origin, obtained from either human or animal donors, or immortalised cells, which can significantly from the native counterparts [8,11,13,14,16,24–26]. Protocols for differentiation of RPE from human embryonic stem cells (hESC; [27,28]) and from hiPSC [28–32]) have been established, and the cells have been successfully cultured or differentiated in mono-culture on a variety of materials by different research groups, including our own [33–38]. hESC- and iPSC-derived EC have also been established and compared to the native counterparts [39–42]. However, to the best of our knowledge, neither hESC- nor hiPSC-derived ECs have been studied so far as part of *in vitro* co-culture models of RPE and EC.

2. Materials and methods

2.1. Materials

96/04 L-lactide/D-lactide copolymer (PLA96/4) (PURASORB PLD 9620, purified, medical grade, IV midpoint 2.0 dl/g) was from Corbion, Purac, Netherlands. Dioleoyl phosphatidylethanolamine (DOPE) was from Sigma, Japan. Collagen type IV from human placenta was from Sigma-Aldrich (USA).

2.2. Preparation of porous films

Porous films were generally prepared by the BF method using PLA96/4 as the polymer [20]. Solutions containing 10 mg ml^{-1} PLA96/4 and 1 mg ml^{-1} DOPE were initially prepared in chloroform. Three batches of films were prepared thereafter, following prior optimisation of the casting conditions, intended as a means to manipulate the porosity of the films on the bottom surface. All films were prepared by casting the solution on top of a round cover glass (Ø 12 mm) centrally placed inside a petri dish (Ø

40 mm, Steriplan®). For Batch 1 (designated BF1), 0.8 ml of distilled water was previously added to the petri dish, in order to ensure immersion of the cover glass, and the petri dish was kept at −20 °C until use. Casting was performed by adding 0.3 ml of the polymer/DOPE solution on top of the frozen cover glass. For Batch 2 (designated BF2), similar conditions were employed with the exception of the fact that the cover glass was pre-immersed in an aqueous dispersion of DOPE (0.05 mg ml^{-1}, prepared by sonication). Casting done by adding 0.2 ml of the polymer/DOPE solution on top of the frozen cover glass. For Batch 3 (BF3), 0.5 ml of the polymer/DOPE solution was directly cast on top of the glass slide (non-immersed), used at room temperature (RT). In all cases, solvent evaporation proceeded under humid airflow (80 ± 3% RH). Prepared samples were thereafter allowed to dry at RT in order to eliminate the water droplets condensed at the surface, and were washed three times with 70% ethanol to ensure complete removal of the surfactant. All samples were kept dry in a desiccator until further use.

2.3. Scanning electron microscopy (SEM)

Morphological features of the honeycomb films were observed by SEM, using a field emission scanning electron microscope (FE-SEM, Carl Zeiss Ultra 55, Germany). Aperture size was 10 µm and the acceleration voltage was 1 kV. Dry samples were imaged on top and bottom surfaces.

2.4. Water contact angle (WCA) measurements

The wettability of the porous materials was assessed by measuring the left and right static water contact angle using an optical tensiometer (Attension Theta Lite, Biolin Scientific AB, Stockholm, Sweden). A droplet of deionised water (3 µl) was applied to the sample surface using the instrument's automated liquid dispenser. Collected images of the droplets were analysed using the OneAttension software, Version 3.2. Mean values of WCA were calculated from both left and right WCA, and from a minimum of 5 measurements per sample type (2–3 independent batches).

2.5. Electrical resistance (R)

The electrical resistance (R) across the porous films was measured to assess the permeability of the materials, generally as described in our previous work [19]. Samples were firstly pre-immersed in DPBS overnight in order to ensure soaking. After that, samples were mounted into P2307 sliders (Physiologic Instruments, USA) and tightly assembled to a custom-built Teflon chamber, where contact between two compartments containing DPBS was made through a small circular opening containing the sample (Ø = 0.031 cm^2). R values across the materials were measured using an EVOM 2 Epithelial Voltohmmeter (World Precision Instruments, USA). Measurements across the empty sliders, where contact between the two compartments of the Teflon chamber was maintained by the uncovered opening, were similarly carried out, in order to establish the reference for the maximum R. Mean R values were determined from six measurements obtained from a minimum of 3 independent batches.

2.6. In vitro *stability of BF films*

The stability of the porous films *in vitro* was investigated by incubating the materials in phosphate buffered saline (PBS) pH 7.4 at 37 °C. Degradation studies were carried out using three independent sample batches per time point. Briefly, samples with a diameter of 12 mm were initially washed with 70% ethanol in order to eliminate any residues caused by sample preparation. Samples were left to dry at RT overnight. After that, samples were placed in a vacuum chamber for a minimum of four hours in order to ensure that all water had been removed. After measurement of the initial dry mass (m_i), samples were individually placed inside the wells of 6 well-plates, to which 6 ml of PBS were added per well. The plates were placed in the incubator either for 3 or 5 weeks. PBS solution was replaced once a week. Finally, samples were removed from the wells, and were thoroughly washed with distilled water. Samples were left to dry overnight, and further in the vacuum chamber as described above, before determination of the final dry mass (m_f). Total mass loss after the degradation study was estimated from the equation:

$$Mass\ loss\ (\%) = \left[\frac{(m_i - m_f)}{m_i}\right] \times 100$$

2.7. Deposition of Langmuir–Schaefer (LS) films of collagen

Collagen type IV was treated as described before [19,35]. Briefly, collagen was first dissolved in dilute acetic acid (pH∼3) to a concentration of 1 mg ml^{-1}. The prepared solution was then sonicated in an icy water bath for 10 min, followed by a 10 min rest period, and by an additional 10 min of sonication. A KSV minitrough system was used to prepare the LS films [35]. 2× PBS pH 7.4 (20.8 ± 0.5 °C) was used as the subphase. A glass microsyringe was used to add dropwise 180 µl of the freshly sonicated collagen solution to the subphase. Collagen was allowed to stabilise on the subphase for 30 min before compression at a speed of 65 mm min^{-1}, *i.e.* 49 cm^2 min^{-1}. For the horizontal deposition of collagen type IV on both the top and bottom surfaces of each film, samples were previously stabilised by insertion between two Parafilm® "M" (Bemis, USA) rings. This simple procedure allowed us to carry out the sequential deposition of the Langmuir–Schaefer films on the two surfaces. Deposition was carried out by the touch and lift method at a pressure of 30 mN m^{-1}. Double-coated surfaces were left to dry vertically (in order to avoid contact with the surfaces) in a desiccator. LS-coated films were imaged by SEM, as described above. The topographical features of the LS-coated surfaces were further assessed by Atomic Force Microscopy (AFM), using an XE-100 microscope from Park System Corp, USA (10 × 10 μm^2 scanned area). Surfaces were scanned in noncontact mode at RT, using an APPNANO AFM cantilever (ACTA). Image acquisition and processing was carried out using XEP and XEI software, respectively (Park Systems, USA).

Thickness of the hydrated, double LS-coated films was determined using a contact profilometer (Dektak XT, Bruker, USA; $n \geq 7$). In order to allow sample hydration, samples were pre-immersed in cell culture medium at 37 °C overnight. The excess liquid was removed before carrying out the profilometry measurements.

2.8. Differentiation of hiPSC cells towards endothelial cells

Healthy adult skin fibroblast UTA.04607.WTS hiPSC cells, derived and characterised at Prof. Katriina Aalto-Setälä's laboratory at Tampere University as previously described [43], were used for EC differentiation. No new lines were derived in this study. The hiPSC cells were previously adopted to feeder-free conditions [44]. The EC differentiation method was the modification of Liu et al. [45]. Briefly, the healthy adult skin fibroblast derived UTA.04607. WTS hiPSC cells were seeded as single cell suspension on human recombinant laminin 521 (Biolamina) coated CellBind® 24 well plates (Corning) at densities from 11 000 cells/cm^2 to 52 000 cells/cm^2 in Essential 8™ Flex medium (Gibco). Cells were incubated for 24 h at +37 °C in 5% CO_2 while small colonies formed. The medium was then changed to DMEM/F-12 with GlutaMAX™ (Gibco) supplemented with 4 µM CHIR 99,021 (Tocris). After a two-day

Table 1
FACS antibodies used in flow cytometry analyses. Volume denotes the volume of antibody solution used per one test.

FACS antibody	Manufacturer	Volume (µl)
PE anti-CD144	eBioscience 12-1449-82	1
APC anti-CD31	eBioscience 17-0319-42	1
FITC anti-CD34	ImmunoTools 21270343	5
FITC anti-TRA-1-81	BD Pharmingen 560194	10

incubation period, the medium was changed to Endothelial Cell Basal Medium 2 (PromoCell) supplemented with 5 ng/ml bFGF (Miltenyi) and 10 ng/ml VEGF165 (R&D Systems). After two days, endothelial-like cells were expanded in Endothelial Cell Growth Medium MV2 (PromoCell) supplemented with 10 ng/ml VEGF165, henceforth designated as EC medium. All cell culture conditions in this method include 25 U/ml Penicillin-Streptomycin (Thermo).

2.9. Flow cytometry analysis

Progression of differentiation and characterisation of sorted ECs was assessed by flow cytometry analysis. Endothelial or endothelial-like cells were washed once with DPBS, detached enzymatically using TrypLE™ Select (Gibco) and harvested in 10% FBS (Gibco) in DMEM/F-12 + GlutaMAX™. Cell suspension was passed through a 40 µm mesh strainer before a volume of cell suspension corresponding to 1×10^5 cells was transferred to a 5 ml round bottom tube for each staining. Cells were washed twice with buffer solution (0.5% BSA (Sigma) in DPBS + 4 mM UltraPure™ EDTA (Invitrogen)) and stained with FACS antibodies (Table 1) for 20 min in 50 µl of buffer. Samples were washed twice with buffer solution after staining. Flow cytometry analyses were performed using BD Accuri™ C6 flow cytometer (BD Biosciences) and C6 Software (BD Biosciences).

2.10. Selection and cultivation of the CD31 positive cell fraction

ECs were selected from the undifferentiated cells using MACS CD31 MicroBead Kit (Miltenyi). Cells were harvested as described before and up to 1×10^7 cells were washed twice with buffer solution with the same composition as described before. The cell pellet was resuspended to 60 µl of buffer solution and 20 µl of FCR-block was added. After brief vortexing, 20 µl of CD31 MicroBeads were added, the suspension was vortexed again and was incubated for 15 min at +4 °C, before being washed once with buffer. A MS-column was placed to the MiniMACS separator and cells were sorted according to the manufacturer's protocol.

Selected CD31 positive hiPSC-derived ECs were seeded on Nunc™ on T75 flasks (Thermo) coated with sterile 0.1% gelatin (Sigma) in water, at densities from 2500 cells/cm^2 to 4000 cells/cm^2 in EC medium. Cells were cultured until confluent with medium change every other day. Confluent cultures of ECs were detached as described before and cryopreserved in EC-cryomedium (50% FBS, 40% Endothelial Cell Growth Medium 2 (ECGM-2; PromoCell), 10% DMSO (Sigma)) [45]. hiPSC-derived ECs were cultured for other applications, the same way as described here, in different formats. Human retinal microvascular ECs (ACBRI-181; Cell Systems) were cultured the same way for all assays.

hUVECs were previously extracted at BioMediTech, Tampere University from the umbilical cords acquired from scheduled Caesarean sections according to [46]. Culture of the hUVECs was carried out according to [46,47], if not stated otherwise.

Human adipose stem cells (hASCs), used for the angiogenesis assay (in Section 2.13), were also extracted at Tampere University, from adipose samples acquired from surgical procedures, according to [46]. Culture of the hASCs was performed according to [47].

Table 2
List of primary and secondary antibodies used for immunofluorescence labelling of ECs.

Primary antibodies	Manufacturer	Host	Dilution
anti-von Willebrand factor	Dako A0082	rabbit	1:400
anti-CD31	Dako M0823	mouse	1:400
anti-CD144	BD biosciences 555661	mouse	1:400
Secondary antibodies	**Manufacturer**	**Host**	**Dilution**
Alexa Fluor™ A488 anti-rabbit	Invitrogen A21206	donkey	1:500
Alexa Fluor™ A568 anti-mouse	Invitrogen A10037	donkey	1:500

2.11. Indirect immunofluorescence labelling of ECs

The hiPSC-derived ECs were cultured on Nunc™ 96-well plate as described before until confluent. For indirect immune staining, cells were washed once with PBS, fixed in 4% paraformaldehyde for 10 min, permeabilised in 0.1% Triton X-100 for 10 min and blocked in 3% BSA for 1 h. Cells were stained with endothelium-specific primary antibodies anti-von Willebrand Factor (vWF), anti-CD31 or anti-CD144 (Table 2) in 0.1% BSA for 1 h at RT or overnight at +4 °C. Secondary antibodies (Table 2) were also diluted in 0.1% BSA and the cells were stained for one hour at RT. Samples were mounted, and the nuclei visualised using Vectashield (Vector Laboratories). hUVECs and ACBRIs were used as positive controls. The cells were cultured and labelled the same way as hiPSC-derived ECs. Stained samples were imaged using an Olympus IX51 Fluorescence microscope (Olympus).

2.12. Acetylated low-density lipoprotein uptake assay

Functionality of differentiated ECs was analysed by assessing the uptake of acetylated LDL using Dil-Ac-LDL (Cell Applications). hiPSC-derived ECs were cultured on Nunc™ 96-well plate as described before until confluent and stained according to manufacturer's protocol. hUVECs and ACBRIs were used as positive controls. The cells were cultured and labelled the same way as hiPSC-derived ECs. Stained samples were imaged using an Olympus IX51 Fluorescence microscope (Olympus) and the acquired greyscale images were colourised using Adobe Photoshop CS4 (Adobe).

2.13. Angiogenesis assay

The angiogenetic capacity is an important characteristic of ECs. The 3D capillary formation is a complex process. The mesodermal support, for example from the hASCs, has been shown to improve reproducibility and formation of capillary network [47,48]. Here, the angiogenic capacity of hiPSC-derived ECs was assessed with hASCs co-culture [47] with slight modifications. Lab-Tek™ (Thermo) 8-well Chamber Slides™ were coated with 0.1% gelatin. hASCs were seeded at 20 000 cells/cm^2 in ECGM-2 and incubated for 2–3 h to establish adhesion to the well surface. hiPSC-derived ECs, hUVECs and ACBRIs were seeded on top of hASCs at 8000 cells/cm^2. Slides were incubated for seven days with one medium change at day three. Indirect immunofluorescence labelling of co-cultures was performed as described earlier. ECs were stained for rabbit anti-von Willebrand factor (1:400, A0082, Dako) and formation of basement membrane was assessed by staining for goat anti-collagen IV (1:100, AB769, Millipore). Secondary antibodies used were Alexa Fluor™ anti-rabbit A488 (1:500, A21206, Invitrogen) and Alexa Fluor™ anti-goat A568 (1:500, A11057, Invitrogen). Structures were imaged using Zeiss LSM700 laser scanning confocal microscope and Zeiss 2.1 Black software.

2.14. Processing the honeycomb films for cell culture

Honeycomb films were UV-treated in a laminar hood for 20 min per side. Then the material was cut into four segments and each segment was clamped between PermeaSys Base element (Code HS1-BL) meant for thin materials samples and Holder lid (Code HS-LP) (Produced at Tampere University, BioMediTech, https://biomeditech.fi/permeasys-holder-set/) that were previously washed twice with 80% EtOH and dried in abs. EtOH. The supporting Parafilm® surrounding the material was removed before sealing the holders by closing with the Closing/ opening tool (Code HS-TO). Holders were stored in 24-well plates in RT until the next day.

2.15. Differentiation and culture of human induced pluripotent stem cells to retinal pigment epithelial cells

The UTA04311.WTs iPSC were differentiated towards retinal epithelial cells as previously described [44] without induction. Briefly, the undifferentiated hiPSCs were dissociated from colonies with TrypLE™ Select Enzyme (Gibco, Thermo Fisher Scientific). Detached cells were transferred to Corning® Costar® Ultra-Low attachment plates, and grown in KnockOut™ Dulbecco's modified Eagle's medium (DMEM) supplemented with 2 mM GlutaMAX™, 1% MEM non-essential amino acids, 0.1 mM 2-mercaptoethanol, 20% KnockOut™ SR (KO-SR) and 50 U/ml penicillin-streptomycin (all from Gibco, Thermo Fisher Scientific). An overnight blebbistatin (5 µM, Sigma-Aldrich) supplementation of the medium was utilised to improve embryoid body (EB) formation. Thereafter the spontaneous RPE differentiation was induced by reducing the KO-SR to 15%, and this medium is referred thereafter as DM-. The EBs were allowed to mature for 4 days. Pigmented areas were manually separated with a scalpel and dissociated with TrypLE™ Select Enzyme, and acquired single cell suspension filtered through 100 µm BD Falcon cell strainer (BD Biosciences, San Jose, USA), and replated onto well plates coated with human 10 µg collagen IV (COLIV; Sigma-Aldrich, USA) and 1.8 µg laminin (L521; Biolamina, Sweden) to expand cell numbers and purify the cell population. To expand and purify the culture, this replating was repeated after 42 and 12 days. During this period, DM- medium was replenished thrice a week. After expansion of cells (passage 4), the hiPSC-RPEs were dissociated with Trypsin–EDTA, filtered through a strainer and stored to cryo bank in LN2. One week before the start of the experiments, the batch of mature hiPSC-RPE cells was thawed from liquid nitrogen. To ensure the viability of thawed cells, the mature hiPSC-RPE cells were plated on 10 µg COLIV- and 1.8 µg L521-coated wells at a density of 200,000 cells/cm^2 and allowed to grow for 7 days in DM-.

2.16. Seeding hiPSC-ECs and hiPSC-RPE cells on opposite sides of the films

Co-culture studies were carried out in an 'open' system, where cells cultured on opposite sides of films shared the same cell culture medium. The 10 µl of EMV2 supplemented with 16.6 ng/ µl VEGF (thereafter called as pan-EC medium) was added to the upper side of the apertures to moisten the material. PermeaSys holders with clamped material were flipped upside down and 150 µl of same medium was added to the bottom of the well to moisten the material from both sides. ECs (hiPSC-EC, ACBRI181, hUVEC) were trypsinised and suspended in the pan-EC medium. ECs were seeded on the biomaterials at a concentration of 100,000 cells/cm^2 in 20 µl of pan-EC medium. Cells were let to adhere in small medium volume for four hours. Thereafter, an additional 750 µl of pan-EC medium was added to submerge the PermeaSys holders.

After overnight culture, the PermeaSys holders with plated ECs were flipped such that the ECs were facing down. Excess of medium was aspirated such that the only ECs were left submerged (approximately 200 µl was remaining). The hiPSC-RPE cells, which had been thawed seven days prior the experiment, were then trypsinised, counted and tested for viability. These hiPSC-RPE cells were seeded on the top (honeycomb) side at the concentration of 100,000 cells/cm^2. This equals to 3400 cells/PermeaSys holder aperture in 5 µl volume of medium. hiPSC-RPE cells were let to adhere for eight hours in the incubator. Thereafter the medium volume was increased by adding an additional 50 µl of DM- on the top holder aperture. On the next day, medium was replenished. To prevent formation of air bubbles underneath the holder, approximately 100 µl of the old medium was left unaspirated. Then 1 ml of fresh medium with 2/3 of DM- and 1/3 of pan-EC medium was added to the cultures. Cells were cultured for three weeks because at that time point the hiPSC-RPE cells start to exhibit RPE-features such as the more compacted cobblestone morphology, whereas the films were still intact enough to be liberated from the PermeaSys holders, allowing further analysis. The medium was replenished thrice a week for a three-week cultivation period. There were two biological replicates and two technical replicates of each cell and material combination.

2.17. Indirect immunofluorescence staining of hiPSC-EC and hiPSC-RPE cultures on the biomaterials

After the three-week cultivation period, the biomaterial cultures were gently washed with 1xPBS, fixed 10 min in 4% PFA, permeabilised in 0.1% Triton X-100 for 10 min and blocked in 3% BSA for one hour at RT. The cultures were stained with endothelial-cell specific rabbit vWF (DAKO 1:400) and RPE-specific antibody against cellular retinaldehyde-binding protein (CRALBP, Abcam 1:500) overnight at +4 °C. After three washes with 1xDPBS the same secondary antibodies and staining times were used as in Section 2.11. The biomaterials with cultured cells were carefully liberated from the PermeaSys holders with PermeaSys opening/closing tool. The fragile culture was transferred to drop of Vectashield with DAPI mounting media and placed between two Zeiss cover glasses. The imaging of cultures was done using a Zeiss LSM700 laser scanning confocal microscope by scanning the entire depth at once with a 40× lens using 1.0 µm increase.

2.18. Analysis of cell number

The attachment and proliferation of ACBRI181, hUVEC, hiPSC-ECs cultured on the BF1, BF2 and BF3 was determined after three weeks of culture. From the two replicates, five images from randomly chosen areas on each sample with DAPI-stained nuclei were captured using an Olympus IX AxioScope A1 fluorescence microscope with 20x objective. The cell number on each image was counted using the Cell Counter Plugin of the ImageJ image processing and analysis software. All cells on the image were counted. The cell number is presented as cells in cm^2.

Similarly, the attachment and proliferation of ACBRI181, hUVEC, hiPSC-ECs and hiPSC-RPEs in co-cultures on the BF1, BF2 and BF3 was determined after three weeks of culture from two independent samples with two technical replicates. The image analysis was done from two replicates from which four images acquired from randomly chosen areas with DAPI-stained nuclei were captured using the Zeiss LSM780 confocal microscope and a 40× oil immersion objective with 0.6 zoom. From those, four different 100 µm × 100 µm-sized areas (from upper left, upper right, lower left, lower right and middle) were counted using the Cell Counter Plugin of the ImageJ image processing and analysis software. The cell number is presented as cells in cm^2.

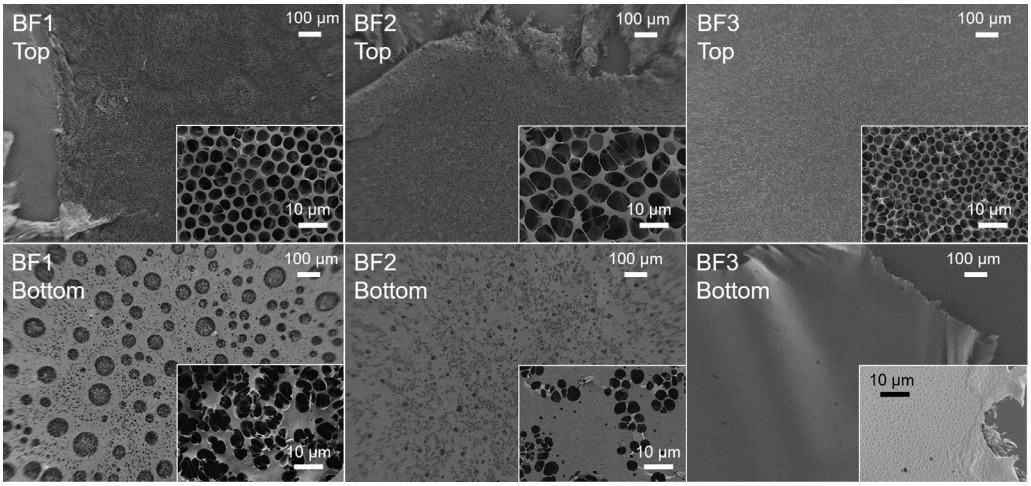

Fig. 1. SEM images showing the surface features of the porous films prepared by the BF method.

2.19. Ethical aspects

The institute has supportive statement from the Ethics Committee of the Pirkanmaa Hospital District to generate hiPSCs from the donor fibroblasts (Aalto-Setälä/R08070) and to use hiPSC lines derived in other laboratories for ophthalmic research (Skottman/R14023). The extraction of human umbilical vein ECs (hUVECs) has the supportive statement from the Ethics Committee of Pirkanmaa Hospital District (Miettinen/R13019). The extraction of hASCs had written patient consent and has the supportive statement from the Ethics Committee of Pirkanmaa Hospital District (Miettinen/R15161).

2.20. Statistical analyses

All numerical data are shown as mean and standard deviation. Statistical analysis of WCA and R was performed by one-way analysis of variance (ANOVA) and the post hoc Games-Howell multiple comparisons test using IBM SPSS Statistics 25 software. The statistical significance of the cell number data was analysed with IBM SPSS Statistics 25 using two-tailed Mann–Whitney *U* test.

3. Results

3.1. Morphology of porous films

The three types of films (BF1–BF3) were imaged by SEM, in order to establish differences in terms of porosity on both top and bottom surfaces (Fig. 1). The top surface was largely characterised by the presence of a uniform array of pores, with only small differences in pore size being observed between samples (BF1 = 4.2 ± 0.4 µm; BF2 = 6.0 ± 1.0 µm; BF3 = 3.4 ± 0.6 µm). In contrast, modifying the casting substrate caused measurable differences in the morphology of the bottom surface of the films, as seen in the second row of Fig. 1. Casting the polymer solution onto the ice substrate led to the formation of large, circular areas (Ø = 56 ± 22 µm) characterised by lower film thickness and wide presence of smaller pores, seemingly in close contact with the top surface (BF1 Bottom, Fig. 1). Maximum distance between these circular areas was often not larger than 30 µm (average = 32 ± 19 µm). Apart from these areas, pores of smaller diameter were generally broadly distributed across the whole bottom surface of BF1 (Ø = 0.5–5 µm). Interestingly, when the polymer solution was cast onto the frozen DOPE solution (BF2), the large circular areas were mostly absent, even though the bottom surface was still extensively porous (Ø = 0.5–5 µm). Both BF1 and BF2 contrast significantly with BF3 (prepared by casting directly on glass), as the bottom surface of the BF3 was noticeably flatter and contained significantly smaller pores (Ø = 1.5 ± 0.7 µm; BF3 Bottom, Fig. 1). Thickness of all samples was approximately 10 µm, as shown by the SEM images presented as Supplementary Material (SM1).

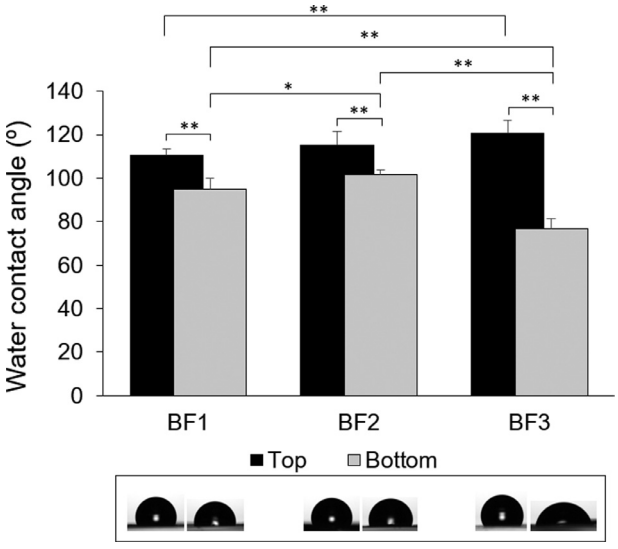

Fig. 2. Water contact angle ($n \geq 10$) measurements. $^{*}p < 0.01$; ** $p \leq 0.001$. Representative photographs of the water droplets at the surface of each sample are shown in the lower panel.

3.2. Water contact angle

Water contact angle (WCA) was measured on the uncoated top and bottom surfaces of BF1-BF3, in order to determine if the different porosity created by the different casting methods had an impact on surface wettability. The results are shown in Fig. 2.

Top surfaces generally had similar WCA, in the average range 111–121°, with differences being statistically significant only for the comparison between BF1 and BF3 ($p < 0.001$). WCA of bottom surfaces (77–102°) was significantly lower than the WCA of top surfaces for all three materials ($p < 0.001$). The most striking observation in the WCA measurements is the fact that

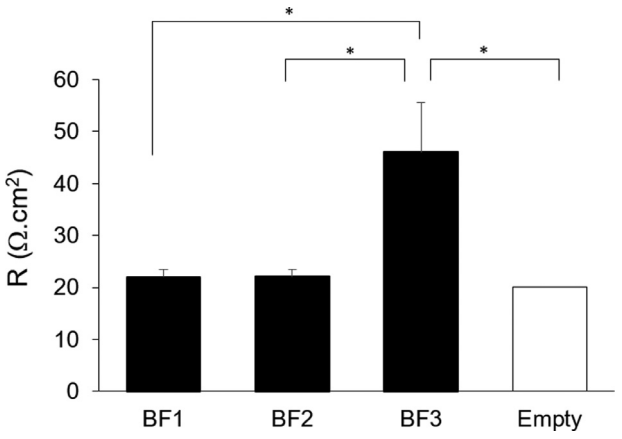

Fig. 3. Electrical resistance (R) across the honeycomb films, and across the empty slider ($n = 6$). * $p \leq 0.005$.

Table 3
Estimated mass loss following *in vitro* degradation studies at 37 °C.

Sample	3 weeks	5 weeks
BF1	3.0 ± 1.3%	3.6 ± 2.7%
BF2	2.7 ± 0.8%	4.4 ± 1.6%
BF3	3.6 ± 3.9%	6.3 ± 3.6%

the different casting methods caused an important effect on the WCA of the bottom surfaces, with the highest value being observed for BF2, followed closely by BF1. WCA of the bottom surface of samples cast directly on glass (BF3) was the lowest among all surfaces (77 ± 5°), as clearly shown also by the microscopy images of the drops beneath the graph in Fig. 2.

3.3. Electrical resistance

Results of electrical resistance (R) across the porous materials are shown in Fig. 3. No significant differences were found between the materials that were cast on the frozen substrates (BF1 and BF2). In addition, R across these samples was only slightly higher (but not statistically different) than R across the empty sliders, used as control for maximum diffusion. However, R values across BF3 were found to be significantly higher than the other two samples and the control ($p \leq 0.005$).

3.4. Degradation study

Honeycomb films were found to be very stable during the *in vitro* degradation study. The estimated mass loss values are shown in Table 3. Even after five weeks, mass loss was small, with average values being lower than 7% for all three samples.

3.5. Deposition of collagen LS films

Collagen IV LS films were homogeneously deposited onto both top and bottom surfaces of BF1, BF2 and BF3 (Fig. 4(A)). The deposition of the LS film created smooth surfaces, and the pores were found to be completely covered by the collagen layer. SEM images taken from the film edges (*e.g.* top surface of BF1) and from areas that had been cut during sample preparation for SEM (*e.g.* top surface of BF2) clearly show the low thickness of the collagen layer and the nicely organised honeycomb array underneath. Topographical assessment by AFM (Fig. 4(B)) confirmed that the LS films effectively covered the pores. Even so, the topography of the honeycomb surface could still be detected, suggesting that the collagen LS films were very thin and flexible. The depth of the pores was significantly reduced to the nanometre-scale.

Thickness of the pre-immersed double-coated honeycomb films, estimated by profilometry, was found to be 10 ± 1 µm, 13 ± 2 µm and 7 ± 3 µm, respectively for BF1, BF2 and BF3. Despite the overall small range of values, statistically significant differences were found when BF3 was compared to BF1 ($p = 0.005$) and BF2 ($p < 0.001$).

3.6. Characterisation of hiPSC-ECs

The hiPSC which were induced to differentiate towards ECs were carefully characterised. The change from Essential 8 flex medium to first differentiation medium induced cell death and the remaining cell density affected the overcome of the differentiation. If there were too few cells in loose colonies at day two, no differentiation occurred; also seeding densities lower than 16 000 cells/cm^2 resulted in no endothelial type differentiation. However, when the seeding density was 16 000 cells/cm^2 or higher, the cells expressed two different growth patterns. In the first pattern, the cells started proliferating vigorously after day two and only small oval colonies of endothelial-like cells had formed at day four (Fig. 5(A) and (D)). The percentage of differentiated cells was low, with the mean differentiation efficiency at day four being only 2% of all cells analysed with flow cytometry, but high total cell count compensated this. In the second pattern, cells proliferated in a more controlled manner resulting in larger colonies of endothelial-like cells, which emerged and expanded during the differentiation (Fig. 5(B)). In this second one, the total cell count was lower, but the differentiation efficacy was considerably higher, 38.5%. When the first seeding density was 53 000 cells/cm^2 or above, no endothelial-type differentiation occurred. If the culture of endothelial-like cells was extended over the six days the undifferentiated cell population appeared to constrict the expansion of differentiated cells. For that reason, differentiation was terminated at day six and cells were sorted. The sorted and cultured hiPSC-derived ECs displayed common EC morphology (Fig. 5(C) and (F)).

In flow cytometry analysis, all samples were gated for the total live population of cells. Both hiPSC-derived ECs and control cells were double-positive for CD31 and CD144 (Fig. 5(G)) but the co-expression of CD34 and CD31 was found to be different between the primary and differentiated cells (Fig. 5(H)). The primary cells expressed lower levels of CD34 than hiPSC-derived ECs. The pluripotency marker TRA-1-81 was expressed in differentiated cells by less than 1% of the population (data not shown).

The expression of EC surface markers was verified with flow cytometry analysis. Expression of CD31 (Fig. 5(I)) and CD144 (Fig. 5(J)) was prominent in hiPSC-derived ECs but expression of vWF was low in hiPSC-derived ECs compared to control cells.

The maturation and functionality of hiPSC-ECs was verified in Ac-LDL uptake (Fig. 5(K)) and angiogenesis (Fig. 5(L)) assays mimicking the functionality of primary cells. An important characteristic of ECs is the capability of acetylated-LDL uptake [45,49]. In the Ac-LDL uptake assay, hiPSC-derived ECs were able to uptake Ac-LDL as well as control cells (Fig. 5(K)). In addition, formation of capillaries is a typical endothelial feature. When hiPSC-EC or primary ECs were cultured on hACs, all ECs formed three-dimensional, branching tubular vascular structures with distinguishable basal membrane the same way as primary control cells (Fig. 5(L)).

3.7. Cultivation test with EC mono-cultures and EC-RPE co-cultures

The compatibility of the coated porous films as substrates for the cultured cells was firstly evaluated by assessing cell adherence and morphology. Three different EC types were analysed, namely

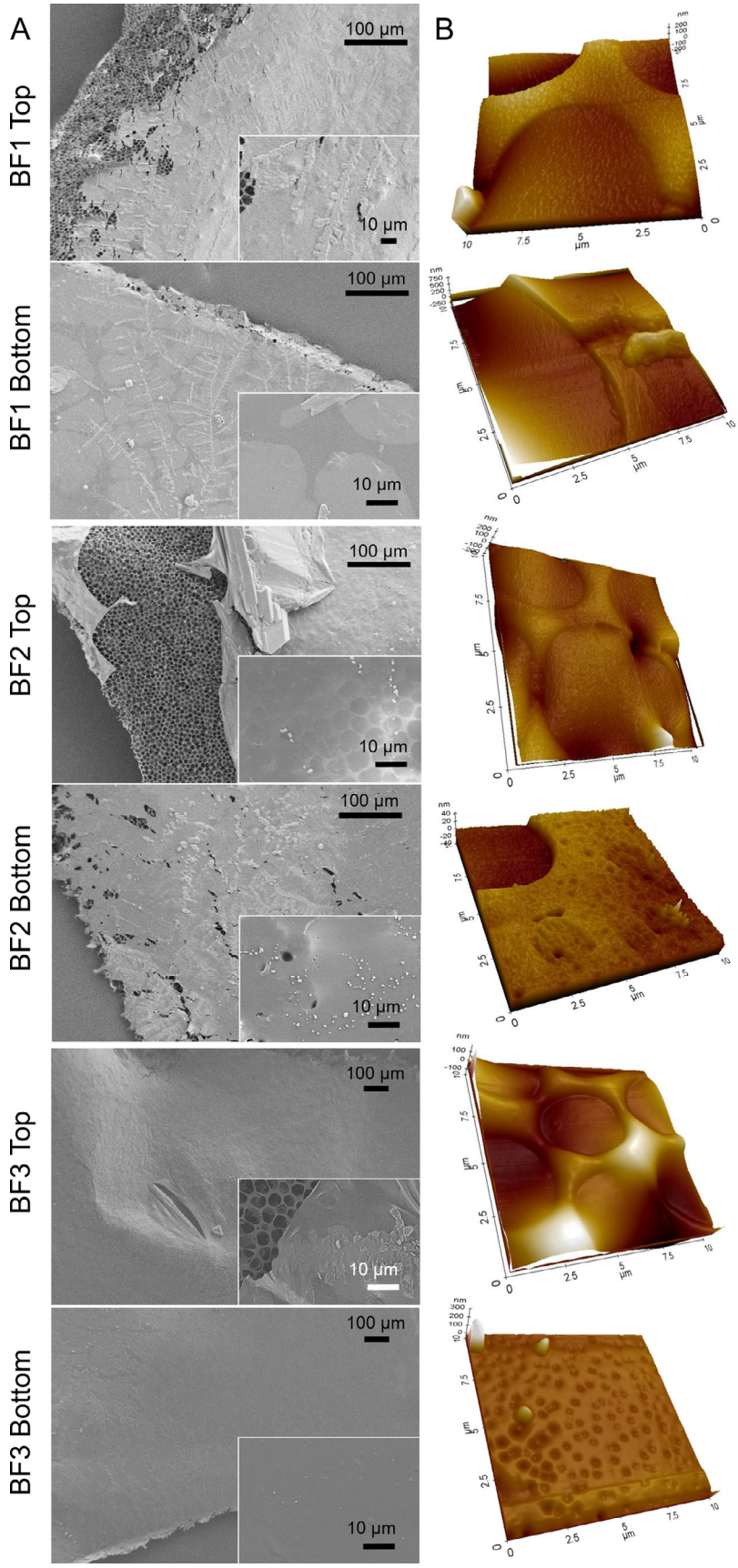

Fig. 4. SEM (A) and AFM (B) images of top and bottom surfaces of honeycomb films double-coated with collagen IV LS films.

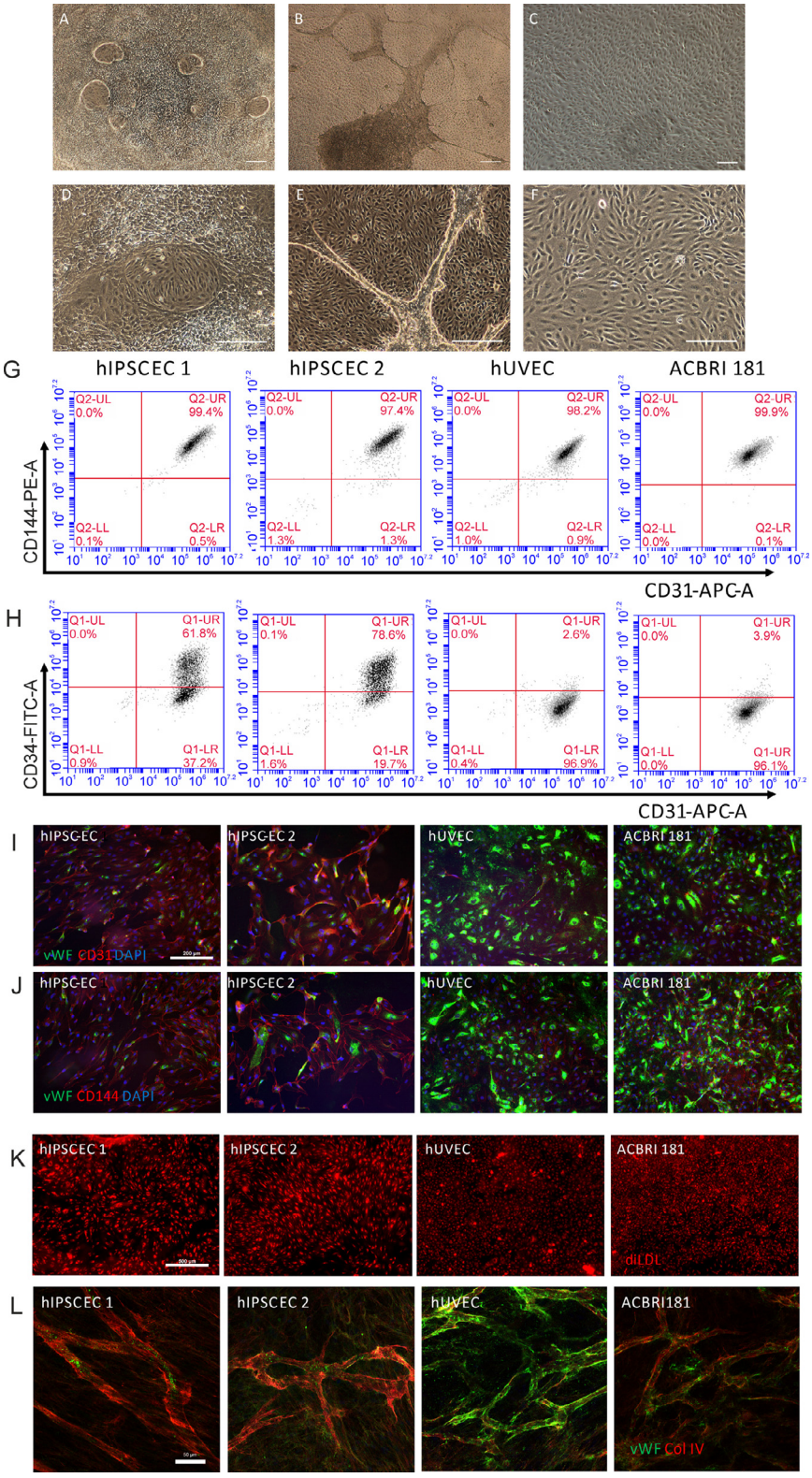

Fig. 5. Characterisation of hiPSC-ECs. Colony morphology of differentiating hiPSC-ECs and post-sort ECs in phase contrast microscopy. Small circular colonies of endothelial-like cells emerged at day 4 during the differentiation (A, D). When cell growth followed different pattern larger colonies of endothelial-like cells were present at day 4 (B, E). CD31 positive sorted cell fraction exhibited endothelial like cell morphology at day 5 post sorting (C, F). Imaged using Nikon Eclipse TE 2000-S microscope and NIS-Elements 4.30.00 software (Nikon). Scale bar 200 µm.

Comparison of hiPSC-derived ECs' and primary ECs' expression of vascular endothelial markers in flow cytometry analysis (G). Comparison of hiPSC-derived ECs' and primary ECs' expression of vascular endothelial markers by indirect immunofluorescence labelling. Sorted and cryopreserved ECs were cultured for two days as described before and labelled with endothelial surface markers CD31(red, I), CD144 (red, J) and vWF (green). hiPSC-derived ECs express junctional CD31 and CD144 prominently but expression of vWF is distributed to only a fraction of the cells as all control cells had significant vWF expression (I, J). Scale bar 200 µm. Confluent EC cultures were exposed to DiI-labelled Ac-LDL for 4 h and imaged hiPSC-derived ECs are capable of Ac-LDL uptake. Scale bar 500 µm. (K). hiPSC derived ECs are capable of forming vascular structures when co-cultured with hASCs. Confocal images of hASC-EC co-cultures at day seven. ECs visualised using vWF (green) and basal membranes using collagen IV (Col IV; red) (L). Scale bar 50 µm. (For interpretation of the references to colour in this figure legend, the reader is referred to the web version of this article.)

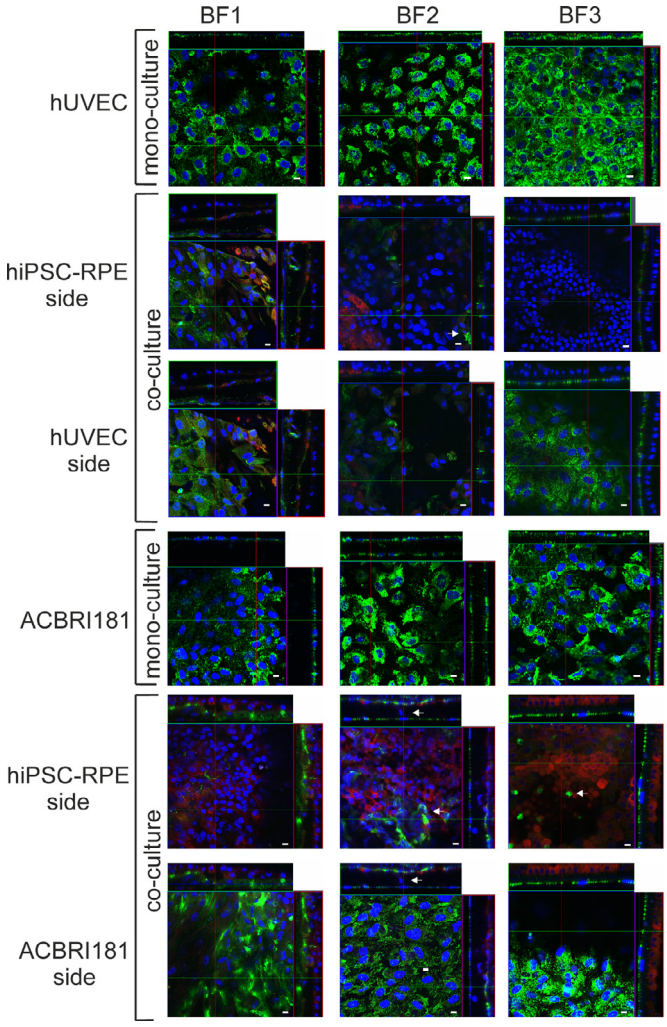

Fig. 6. Representative confocal micrographs from biomaterial culture tests (BF1–BF3) with hUVEC and ACBRI181, cultured as a mono-culture, or in co-culture with hiPSC-RPE. Endothelial cells were cultured in all cases on the bottom side of the films. The co-cultures are visualised from the EC side, and the hiPSC-RPEs from the same cultures but from opposite sides. Samples were immunostained with the RPE-specific marker CRALBP (red) and endothelial cell-specific vWF (green). Nuclei were counterstained with DAPI (blue). The white arrows denote cells migrating across the biomaterial and vWF positive cells in-between the CRALBP positive cells. Scale bars 10 μm. (For interpretation of the references to colour in this figure legend, the reader is referred to the web version of this article.)

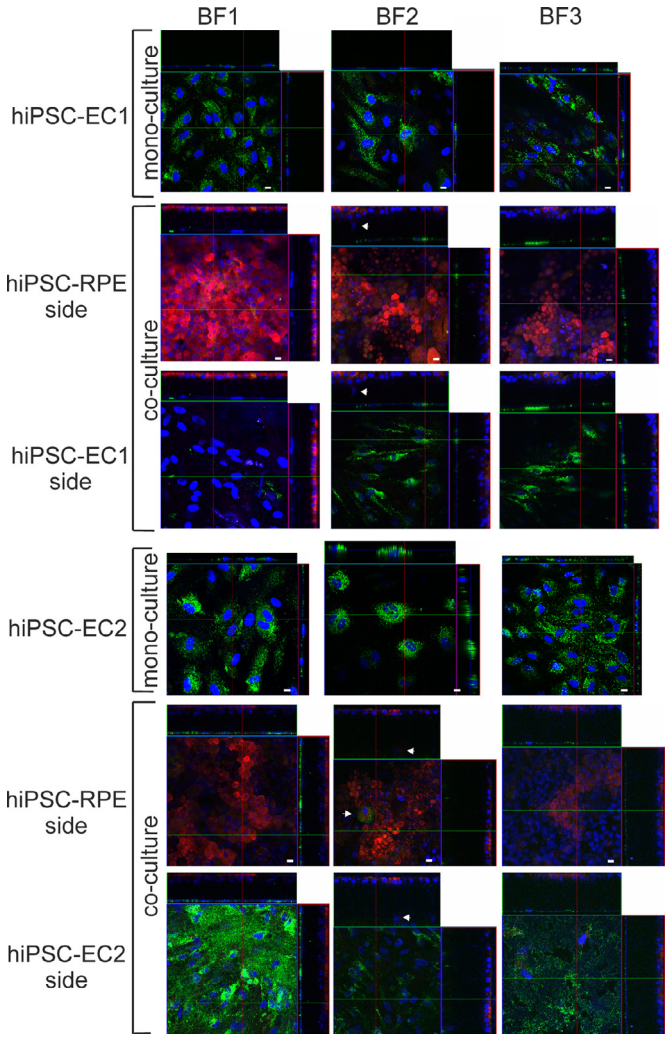

Fig. 7. Representative confocal micrographs from biomaterial culture tests (BF1–BF3) with hiPSC-EC, cultured as a mono-culture, or in co-culture with hiPSC-RPE. Endothelial cells were cultured in all cases on the bottom side of biomaterial. The co-cultures are visualised from the EC side, and the hiPSC-RPEs are from the same cultures but from opposite sides. Samples were immunostained with the RPE-specific marker CRALBP (red) and endothelial cell-specific vWF (green) Nuclei were counterstained with DAPI (blue). The white arrows denote cells migrating across the biomaterial. Scale bars 10 μm. (For interpretation of the references to colour in this figure legend, the reader is referred to the web version of this article.)

pluripotent stem cell derived-ECs (hiPSC-EC), and two different primary ECs (hUVEC and ACBRI181), and by co-culturing ECs and hiPSC-RPEs on opposite sides of the same material. ECs were cultured in all cases on the bottom side of the material. Cells in co-culture were allowed to contact through the pores of the biomaterial, and through the shared cell culture medium.

The commonly used ECs, hUVECs, formed confluent cultures when grown in mono-cultures (Fig. 6). All materials supported the adherence of hUVECs. The pores, seen in BF2 (Fig. 6), were devoid of hUVEC cells. In hUVEC and hiPSC-RPE co-cultures (Fig. 6), the morphology of hiPSC-RPE cells was elongated. On BF2, the hUVECs were occasionally found on the hiPSC-RPE side (pointed with the white arrow). In mono-cultures, the retinal primary cells, ACBRI181, performed similarly as the hUVECs (Fig. 6) in forming homogenous vWF positive layer of cells. The RPE cells in their native form grow in monolayers. In ACBRI181 and hiPSC-RPE co-cultures, however, it was evident that for BF1 the hiPCS-RPE cells were growing multi-layered. When the cells were seeded on the biomaterial the collagen IV layer prevented cells from getting inside the pores of the biomaterial. After the three weeks of culture there were nuclei in between of the biomaterial (see white arrow) which were taken an indication of cell migration in BF2. In addition, there were vWF-positive ACBRI181 cells in between the hiPSC-RPE cells, which was the second indication of migration of endothelial cells though the biomaterial. The less porous BF3 material exhibited the highest CRALBP staining on the hiPSC-RPE cell edges, suggesting that BF3 supported the maturation of hiPSC-RPE cells better than BF1 or BF2 in ACBRI primary retinal endothelial co-cultures.

Culturing tests were carried out using three different batches of hiPSC-ECs, but as they all performed similarly, only two are shown in Fig. 7. Both hiPSC-EC1 and hiPSC-EC2 formed an even monolayer of vWF-positive cells. The coverage of hiPSC-EC cells (Fig. 7) was lower than with the primary ECs (Fig 6). In co-cultures, the hiPSC-EC1 cells were slightly smaller than hiPSC-EC2 cells. In the beginning of the culture, the collagen IV coating prevented the cell from getting to the pores of films. As described above for BF2 specifically, the detection of cell nuclei within the

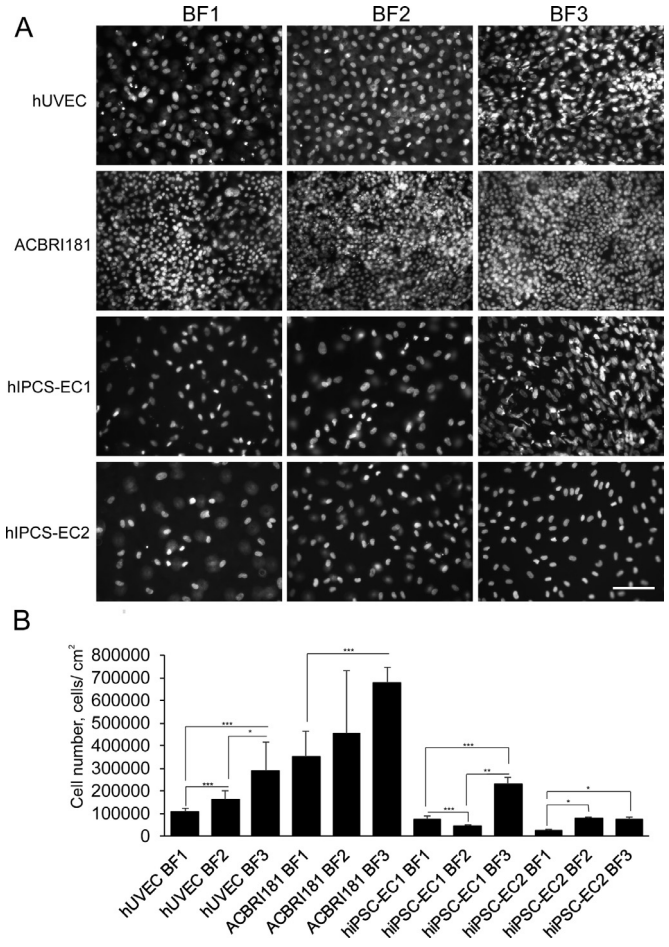

Fig. 8. Number of hUVEC and ACBRI181 cells, and hiPSC-EC in mono-cultures grown on the different biomaterials (BF1, BF2, BF3). The number of cells, *i.e.* DAPI-stained nuclei, was evaluated from wide field micrographs. Representative images of nuclear stain DAPI used for endothelial cell number analysis (A). Scale bar 100 μm. Cell number analysis after three weeks of culture on BF1, BF2 or BF3 (B). Standard deviation denoted with the error bars. The statistical significance: $^{*}(p \leq 0.05)$, $^{**}(p \leq 0.005)$ and $^{***}(p \leq 0.001)$ indicating the significance between the indicated samples.

biomaterial (see arrowheads) was taken as an indication of cell migration through the pores of biomaterial. In addition, mixing of different cell populations could be detected in the hiPSC-EC2-hiPSC-RPE co-cultures, where vWF-positive cells were in between the CRALBP-positive hiPSC-RPE cells (pointed with white arrow). The hiPSC-RPE cells had the most compact hexagonal structure and highest intensity in CRALBP-staining on BF1 and BF2, which may indicate that those materials provide better support for RPE cell maturation.

From the visual inspection, the number of ECs appeared to vary between different culture materials. To investigate whether there were differences in number of ECs in mono-cultures on different biomaterials, the number of DAPI-stained nuclei was counted with the aid of Image J Cell counter plugin (representative micrographs in Fig 8(A) and calculated values in graph Fig. 8(B)). The primary cells, hUVEC and ACBRI181, generally demonstrated higher cell density than hiPSC-EC (hUVECs 0.1×10^8 to 0.3×10^8 cells/cm^2 and ACBRI181 0.35×10^8 to 0.7×10^8 cells/cm^2 compared to $< 0.2 \times 10^8$ of hiPSC-ECs/cm^2). With all tested ECs the BF1 material had the lowest number of cells compared to BF2 or BF3. This difference was statistically significant in hUVECs and hiPSC-ECs, and in ACBRI181 between the BF1 *vs* BF3 (Fig. 8(B)).

The cell density was analysed also from the co-cultures (Fig. 9). The first important observation is that the number of hUVEC and ACBRI181 cells in mono-culture was, as a whole, significantly reduced in the presence of hiPSC-RPE, whereas the number of hiPSC-EC was mostly unaffected by the presence of the retinal epithelium. In addition, the increase in the primary EC numbers seen in mono-cultures from BF1 to BF2 and from BF2 to BF3 was seen only in hUVEC co-culture but not in ACBRI181. This difference detected in hUVECs was also statistically highly significant ($p \leq 0.001$). In the hiPSC-EC-hiPSC-RPE co-cultures, only BF1 demonstrated a substantially higher number of cells (hiPSC-EC1), and the difference was statistically significant. In addition, the hiPSC-RPE cell number was evaluated from the co-cultures (Fig. 9). The ACBRI181 co-cultures had a substantially lower number of hiPSC-RPE cells ($<0.26 \times 10^8$ cells/cm^2) on BF1, BF2 and BF3 than hUVECs. The highest hiPSC-RPE cell numbers were found for the co-cultures with hiPSC-EC1 and hiPSC-EC2, as there were $>0.3 \times 10^8$ cells/cm^2 on all materials. hiPSC-RPE cell number on BF2 was slightly lower, but statistically significant, than cells cultured on the other two materials ($p \leq 0.001$).

4. Discussion

In this work, we took advantage of the versatility of the BF method to modulate the porosity and permeability across the materials, and thereby influence the contact between cells cultured on opposite surfaces. Casting directly on the glass substrate (BF3) limited pore formation on the bottom surface. It is known that casting on water [50] or ice [51] can lead to the formation of through-pores, but typically low casting volumes are needed, and the resulting films are too thin to be free-standing, requiring transfer onto a secondary support. With this in mind, we prepared BF1 by casting on ice, albeit using a significantly larger volume of casting solution, compared to the previous studies [50,51], in order to ensure that the produced films were self-supporting. As a result, high porosity was observed on the bottom surface, with circular areas of smaller thickness suggesting a close contact with the top surface. It is interesting to note that the addition of DOPE to the frozen substrate, BF2, caused the bottom surface to remain highly porous, but having a more regular pore distribution as compared to BF1. Fukuhira et al. [52] demonstrated that the low hydrophile–lipophile balance (HLB) value and high interfacial tension of DOPE contribute to stabilise the condensing water droplets from the humid environment, enabling the formation of the organised honeycomb pattern [52]. Even so, to the best of our knowledge, frozen aqueous dispersions of DOPE have not been reported before as the substrate for honeycomb film fabrication. It is anticipated that the surfactant present at the ice-polymer solution interface may have contributed to stabilise the formation of water nuclei, acting as templates for the formation of pores on the bottom surface.

Considering that the top surfaces of BF1-BF3 were similarly subjected to the humid environment, with the resulting pore size not differing significantly between samples, it is unsurprising that the WCA values were similar between samples. Differences between the three materials were however confirmed by the WCA measurements on the bottom surface. It is well known that WCA depends on the chemical composition of the surface, as much as it depends on its topography [53,54]. WCA of such porous surfaces as honeycomb films, for instance, is typically higher than that of flat counterparts, due to the formation of air pockets between the rough surface and the water drop [55]. This explains the lower WCA observed for BF3, the flatter bottom surface, as compared to BF1 and BF2. The specific topographical features of the latter two (including diameter, depth and shape of pores, and distance between them) additionally explain the small but statistically significant differences between these samples [54]. Even more

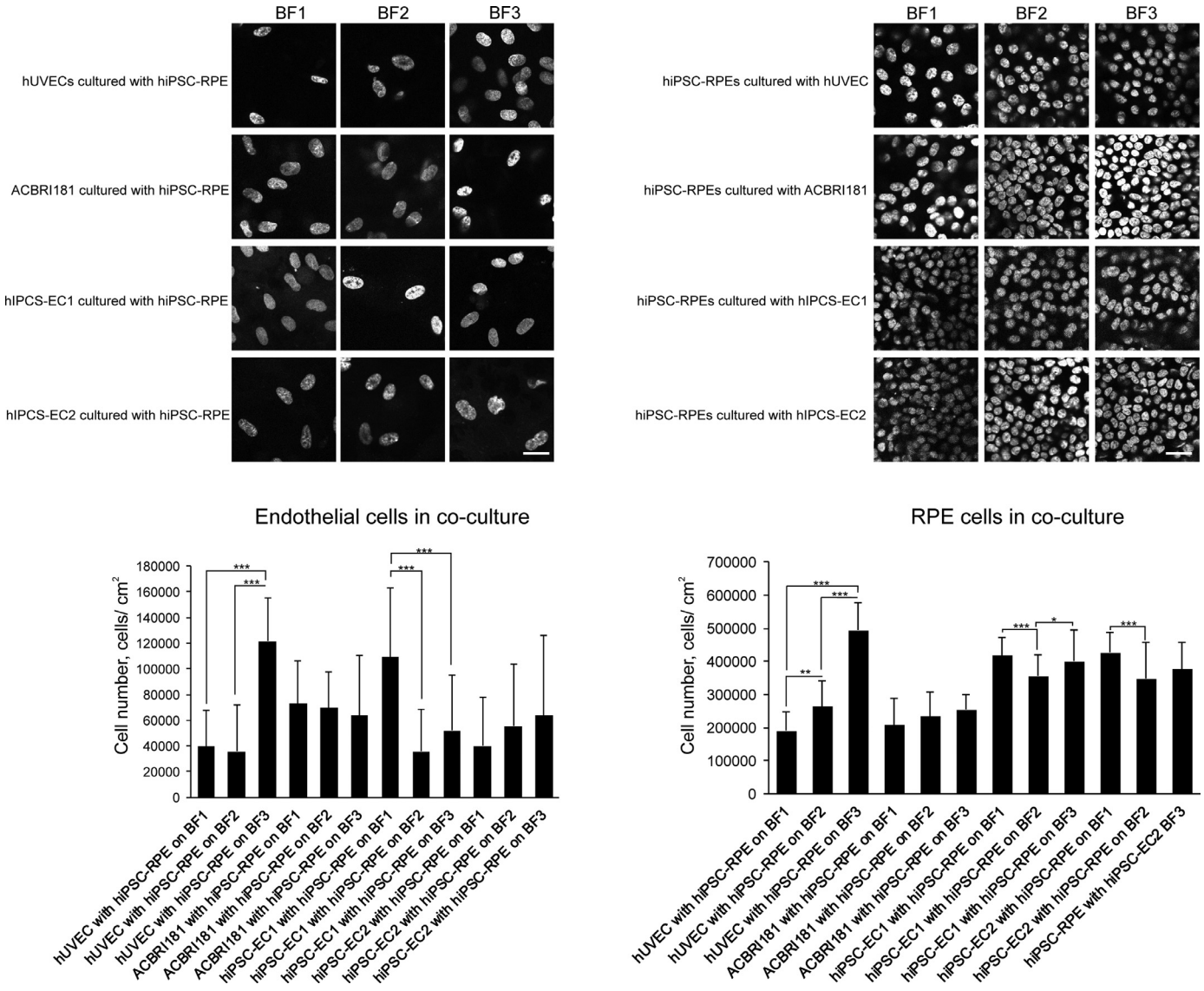

Fig. 9. Number of hUVEC and ACBRI181 cells, and hiPSC-EC in co-cultures with hiPSC-RPE grown on the different biomaterials (BF1–BF3) for three weeks. The number of cells, *i.e.* DAPI-stained nuclei, was evaluated from confocal micrographs. Representative images (100 µm × 100 µm) of nuclear stain DAPI used for endothelial cell number analysis. Scale bars 25 µm. Cell number analysis after three weeks of culture on BF1, BF2 or BF3 (B). Standard deviation denoted with the error bars. The statistical significance: * ($p \leq 0.05$), ** ($p \leq 0.005$) and *** ($p \leq 0.001$) indicating the significance between the indicated samples.

expressively, using the frozen subphases for casting (BF1, BF2) successfully improved the permeability of the films, as shown here by electric resistance, a measurement of the movement of ions across the materials [20]. Taken together, these results suggest that the possibility to manipulate porosity and permeability inherent to the BF method can be particularly advantageous for the development of *in vitro* models of the BRB. In fact, the normally permeable Bruch's membrane becomes significantly less permeable in severe cases of AMD, compromising the availability of nutrients to the neural retina, and the elimination of metabolic waste [56].

Also important in this context is the stability of the materials over time. Previous studies with lactic acid polymers and co-polymers have demonstrated that the degradation rate of the scaffold is inversely related with cell viability and migration into the scaffold [57]. For co-culture of RPE and EC, a fast-degrading material could imply that the two cell types would quickly reach physical contact, which would hinder the intended biomimetic properties of the model. In this work, the high *in vitro* stability of all materials for a period of 5 weeks encouragingly suggests that the materials may also demonstrate high stability *in vivo*, thereby not significantly affecting cells cultured on (or in the vicinity of) the materials. Additional studies should further establish the molecular cut-off of the films, and time-dependent changes *in vivo*.

In order to improve the biocompatibility of the BF films toward cultivation of hiPSC-RPE and hiPSC-EC, both top and bottom surfaces of the honeycomb films were coated with collagen IV LS films. Langmuir films are prepared by spreading amphiphilic species at the air-water interface followed by solvent evaporation or equilibration, and compression at the interface. The compression step causes the molecules to reorient into a compact monolayer, which can be subsequently deposited onto a solid substrate by vertical dipping or horizontal lift of the substrate, thus forming LB or LS films, respectively [58]. Previous research has shown that oriented collagen fibres can be created by compression of the fibres in a Langmuir trough, and that the collagen LB or LS films are favourable substrates for cultured cells [59]. Encouraged by our previous findings on the positive effects of collagen-LS surfaces toward cultured hESC-RPE [19,35], we now embraced the challenge of coating both surfaces of the biomaterials with a thin collagen IV layer on each side. We believe that this is the first work de-

scribing such an approach. The challenges were multifold: (i) the high WCA of PLA96/4 films makes them repel water, preventing immersion in the subphase (thereby precluding the option of vertical dipping for simultaneous coating on both sides, *i.e.* following the LB approach); (ii) the honeycomb films are only ~10 µm, also compromising vertical dipping, and making them fragile materials that cannot be handled with harsh equipment; (iii) the deposition of LS layers on both surfaces implies that direct contact with the surfaces post-deposition should be avoided. Our strategy to sandwich the films between two custom-made Parafilm® "M" rings revealed to be a practical solution to tackle these issues, as the rings made the samples easy to handle, making it possible to sequentially coat both sides of the samples, and providing a stable frame for drying in the vertical position. One of the most fascinating features of collagen IV LS-coated honeycomb films is the fact that the thin collagen layer (previously determined as approximately 30 nm [35]) can cover the pores completely as a contiguous sheet. This contrasts significantly with the results achieved when the samples are coated by simple immersion in the collagen solution, where the pores are typically left exposed [19]. Here as well, both top and bottom surfaces were homogeneously coated. These collagen-LS surfaces can improve cell adhesion and growth for two important reasons: first, the coated surfaces are seen by the cells as nearly flat; secondly, cells are in contact with a biomimetic, continuous sheet of collagen type IV, an important component of the basement membranes of RPE and the choriocapillaris [4]. Furthermore, collagen IV has been suggested to have a role in regulating migration and growth of ECs, and in angiogenesis [60]. Because the angiogenic cascade has been associated with increased secretion and extracellular deposition of collagen type IV [61], we additionally hypothesize that *in vitro* disease models simulating angiogenesis in the retina may be developed using thicker collagen IV LS films.

In flow cytometry our hiPSC-derived ECs had high co-expression of CD31 and CD144 suggesting a good endothelial differentiation [41,45,62]. Here, the expression of CD34 was considerably higher in differentiated ECs (61–79%) compared to primary cells (3–4%). Our findings of CD34 expression coincide with findings of Simara et al. [63]. In their experiments, hiPSC-ECs from three different sources displayed similar elevated levels of CD34 expression (64–92%) compared to primary ECs in flow cytometry analyses. The high CD34 positivity may also indicate that the hiPSC-ECs had not reached maturity at this point. Liu et al. [45] reported that CD34 expression peaked at Day 7 in their 12-day differentiation period and started declining after that. In a recent paper [62], it was shown that hiPSC-ECs had a mixed arterial- and embryonic-like identity with prominent expression of both arterial markers. In immunostaining assays, expression of CD31 and CD144 was not as prominent in hiPSC-derived ECs as in primary ECs [41,45]. Our hiPSC-ECs had less vWF stain than the primary EC, and were much bigger in size than primary ECs, similarly as in a previous publication [62]. The hiPSC-ECs differentiated here were very capable of up-taking acetylated LDL and compared well to results of other authors [45,64]. The angiogenesis assays have been performed on different ECM matrices [45,63,64], and with several cell types such as pericytes [41], and stromal cells such as cardiac fibroblasts [62] and hASCs [47]. Here, the hiPSC-ECs as well as primary ECs were able to form tubular vascular structures with distinct basal membrane when co-cultured with hASCs.

A significant number of studies have shown that the high porosity of honeycomb films can influence the properties of cultured cells, for instance by allowing control of protein adhesion, facilitating cell attachment through hooking of extending filopodia, facilitating nutrient transport and waste elimination, and allowing contact guidance [18]. In tissue engineering, honeycomb films have therefore shown promise in mono-culture of several cell types, including *e.g.* rat cardiomyocytes [65], porcine aortic ECs [66,66], mouse preosteoblastic MC3T3-E1 cells and primary rat osteoblasts [67,68] and human dermal fibroblasts and epidermal keratinocytes [69]. Our recent studies also successfully demonstrated the adhesion and maturation of hESC-RPE on PLA96/4 and polybutylene succinate films prepared by BF [19–21]. In spite this, honeycomb films prepared by BF have rarely been studied as substrates for co-culture systems, with only a few reports available for co-culture of bovine aortic EC and smooth muscle cells (SMCs) [70], and for co-culture systems, where the same cell type (cardiomyocytes or hepatocytes) was cultured on both sides of the honeycomb films [71].

In the outer retina, RPE cells are separated from the choroidal ECs by the Bruch's membrane [6]. As such, we propose here the use of the double-coated honeycomb films as Bruch's membrane substitutes. Considering that the human Bruch's membrane has an estimated thickness of approximately 5 µm [72], determination of material thickness was considered essential. Hydrated double-coated honeycomb films were slightly thicker than the native membrane, in order to ensure that the films would be free standing and could be easily manipulated for cell culture and for the extensive material and cell characterisation experiments described in this work. While this limitation is here acknowledged, it is essential to highlight that the BF method, apart from allowing modulation the porosity, wettability and permeability, also allows customisation of sample thickness, which may be considered in subsequent work.

Via humoral factors, the ECs are known to modulate the RPE cell functionality, improving RPE cell maturation [14,73,74] for example by increasing growth factor secretion [73,74], the RPE cell barrier function [16,73,74] and the RPE-specific gene expression [14]. *Vice versa*, RPE cells in co-cultures have been shown to decrease angiogenesis [14] and increase the intracellular gaps [73,75]. RPE cells are typically obtained human adult [11] or foetal [13] donors, or from animal eyes [13]. Immortalised human cell lines such as ARPE-19 are also widely used due to being more easily available [8,11–14,16], but can differ significantly from the native counterparts in terms of functionality and gene expression, and may respond differently to the environment and/or under stress conditions as compared to the native RPE [24–26]. In a similar manner, EC are typically of primary origin [8,11–13,13,15]. Human umbilical vein endothelial cells (hUVEC) are among the most commonly used model of EC [14] due to their easier availability compared to other types of primary cells, but the cells are available in limited supplies, and pooled hUVEC preparations entail batch-to-batch variations, potentially compromising the reproducibility of the results [76]. In addition hUVECs and are not ophthalmic origin, which can also have an effect on their functionality. According to our knowledge, no previous studies have reported EC and RPE co-culture studies using biodegradable biomaterials, in which both the EC and RPE cells are derived from hiPSCs.

Here, we assessed the cellular adhesion on three different BF structures in endothelial mono-cultures and in endothelial-hiPSC-RPE co-cultures. For comparison, hiPSC-derived EC cultured as mono-culture and in co-culture were compared to the commonly used umbilical vein hUVEC, and to the more representative primary human retinal microvascular EC (ACBRI181). All three tested materials (BF1-BF3) supported adherence of both primary (hUVEC and ACBRI181) and hiPSC-EC derived cells. As previous studies have shown that ECs prefer the rougher surface of films, as compared to a smooth surface [77], it is interesting that the highest density for all EC was generally found on the smoothest and less permeable substrate, BF3. However, it is important to emphasise that the EC were cultured on the bottom surface of the films, which lacks the honeycomb topography investigated in the indicated study. In fact, cell adhesion onto patterned substrates is

well-known to depend on multiple factors, including the size and distribution of pores and the specific pattern of the surface. Even so, considering the absence of another cell type, the results strongly suggest the important effect of the material properties on the adhesion and proliferation of the ECs.

The effect of surface properties on the primary ECs (especially in the case of ACBRI181) was more moderate in co-culture than in mono-culture. In most cases, the trends among BF1-BF3 observed in mono-culture were also different than the ones observed in co-culture. This indicates that the material properties *per se* are not the decisive factor of EC fate, especially in an 'open' co-culture system where the cells shared the same culture medium. In contrast, the presence of hiPSC-RPE had a major effect on primary EC fate, as expressively shown by the overall decrease of EC number (Fig. 9), as compared to the mono-cultures (Fig. 8). The generally lower numbers of EC in the presence of hiPSC-RPE is well in agreement with previous studies that have confirmed a decreased confluency of ECs in the presence of RPE [73,75]. A smaller, but noticeable decrease of hiPSC-ECs was also observed in the presence of hiPSC-RPE, while the effect of material properties was also modest, with the surprising exception of hiPSC-EC1 cultured in BF1. It is possible that multiple factors simultaneously affected this event, which should be clarified in future studies.

For all ECs in general, BF2, which had pores wider than 5 μm (unlike BF1 and BF3), often allowed the cells to cross from the apical side to the bottom side and *vice versa*. The migration was seen by detecting the nuclei in-between the BF2 material and as a mixture of cells with the surface marker of the cell type cultured on that side of the film (Figs. 6 and 7). In spite of the fact that the effects of cell migration in BF2 did not clearly affect the number of ECs in co-culture, it has been discussed that the physical contact of ECs with the RPE cells can mimic the pathological condition occurring in choroidal neovascularisation seen in the wet AMD [78], and that has also been shown to decrease the maturation of RPE cells *in vitro* [79]. The vWF-positive hiPSC-EC2 cells in-between the hiPSC-RPE cells changed the homogeneity of the RPE culture only in the close vicinity.

It is also interesting to note that, in general, higher hiPSC-RPE numbers were found when the cells were co-cultured with hiPSC-EC, as compared to the primary endothelial cells. This suggests a positive effect of these endothelial cells on the pigmented epithelium, and highlights the fact that cells of different origin can exhibit essential differences in behaviour and functionality. Halaidych et al. [62], have previously demonstrated that hiPSC-derived and primary ECs share many similarities such as the similar functional blood vessel formation *in vivo*, but also some differences. The gene expression profile of hiPSC-ECs resemble more embryonic ECs, whereas the marker and gene expression profiles of primary ECs suggest that these are more mature [62,80–82]. For example the vWF expression has been lower in hiPSC-ECs than in primary ECs [62]. Here, we also observed that the intensity of vWF fluorescence was lower in hiPSC-ECs than in primary ECs both in the EC characterisation and in biomaterial cell cultures. Even so, and considering (a) the advantages of hiPSC-derived cells in terms of the possibility to obtain an unlimited number of high quality, specialised cells; (b) that this is the first study on co-culture of hiPSC-EC and hiPSC-RPE; and (c) our preliminary data suggesting that hiPSC-EC favours hiPSC-RPE growth, it is becomes indispensable that additional studies are carried out to reveal the complex biochemical mechanisms that explain hiPSC-EC-hiPSC-RPE interactions, such as gene expression and the influence of secreted growth factors.

In co-culture, hiPSC-RPE cells had more intense CRALBP staining on BF1 and BF2, than on BF3. This was detectable in the primary EC (hUVEC and ACBRI181) co-cultures, but not as prominently as in hiPSC-EC-hiPSC-RPE co-cultures (Figs. 6 and 7). The result suggests that bigger pores, which allow the flux of EC humoral factors, increase the maturation of RPE cells. This is in concordance with the previous studies, which have been carried out with primary ECs [14,16,73,74]. In spite of this, the higher confluency of hiPSC-RPE cells in BF1 than in BF2 or BF3 in hiPSC-EC suggests that BF1 effectively avoids physical contact between the two cell types, while enabling the flow of substances, as seen in the healthy BRB.

In short, differences between mono- and co-culture clearly confirm that ECs and hiPSC-RPE actively influence each other when the cells are in contact through the pores and through the shared medium. Here, we noticed that the endothelial cell co-culture partner influenced the maturation of hiPSC-RPE cells. This highlights the importance of having several different cell types when assessing the effects between cells in co-culture. For the co-culture system relying solely on hiPSC-derived cells, our study demonstrated that the ECs are negatively but moderately affected by the presence of hiPSC-RPE, whereas hiPSC-RPE is less affected by hiPSC-EC than by the primary endothelial cells. For the hiPSC-co-culture system, the results support the idea that the larger pores in BF2 enable endothelial cell migration, mimicking choroidal neovascularization in AMD, whereas the high permeability but lower pore size of BF1 suggest a semi-permeable barrier resembling the Bruch's membrane in the healthy outer retina.

Finally, it is important to acknowledge the challenges of the interpretation of differences among the primary cell lines and hiPSC-EC, and among material types. Here, the modulation of porosity across the material was considered essential, as it can significantly affect the flux of soluble factors secreted by the cells on opposite sides of the material. On the other hand, we successfully extended the scope of the study by investigating the suitability of the new materials as substrates for the three different EC types, especially comparing the iPSC-derived ECs with the most widely studied hUVEC and the ophthalmic counterpart, ACBRI181, both in mono-culture and in co-culture with hiPSC-RPE. It is likely that multiple variables simultaneously contributed to the observed results, including surface topography, material porosity, cell origin, presence/absence of a culture partner, and the presence of an 'open' culture system where the culture medium was shared between the co-cultured cells. Notwithstanding these challenges, this study is an important first step toward the development of optimised materials, which may be partially achieved by modulation of the film preparation conditions by the BF method. Furthermore, the versatility of the LS deposition may allow the preparation of multilayer coatings, closely mimicking the protein composition of the Bruch's membrane. The fact that this is the first co-culture system relying solely on hiPSC-derived cells is particularly encouraging, and up-to-date with the current needs of the scientific community. Future studies using closed systems, *i.e.* where contact between ECs and RPE is exclusively maintained through the pores, may elucidate the specific mechanisms of interaction between the cells. In such circumstances, the modulated properties of the BF films are expected to have highly pronounced effects on the outcome of the cells in co-culture.

5. Conclusions

In this work, we successfully demonstrated that the BF method can be employed to modulate the properties of polylactide honeycomb films, especially in terms of porosity, wettability and permeability. To the best of our knowledge, this was the first attempt to modulate such material properties having in mind the development of a co-culture system for EC and RPE. The materials were thin but self-supporting and demonstrated to be stable *in vitro* for at least 5 weeks. We demonstrated that the deposition of a collagen IV LS layer on both top and bottom material surfaces facilitates the adherence and growth of the three EC types and hiPSC-RPE. Cell attachment and growth tests demonstrated that in

endothelial mono-cultures, smoother and less porous surfaces favoured the growth of primary ECs. Primary ECs are significantly and negatively affected by the presence of hiPSC-RPE in co-culture, while hiPSC-EC are expressively more tolerant to the presence of the co-culture partner than the primary ECs. On the other hand, hiPSC-RPE are much less affected by the presence of hiPSC-EC than by the presence of the primary ECs. The data strongly support the notion that cells of different origin can behave very differently *in vitro* (and expectedly, *in vivo*), which justifies the relevance of parallel studies comparing the different cell types. In co-culture, the effects of material properties on EC behaviour become less prominent than in mono-culture. When cultured together with hiPSC-ECs, hiPSC-RPE seems to benefit from a highly porous substrate (enabling the free flow of substances), but capable of effectively ensuring the barrier properties between the two cell types (*i.e.* avoiding physical contact).

Overall, our results show that this developed co-culture system, based solely on hiPSC-derived cells and on a tuneable biodegradable substrate, holds high promise to simulate the functionality of the outer retina. The versatility of the employed methods allows for further optimisation of material properties, having in mind the design of thinner substrates and/or including multiple components of the Bruch's membrane. Future research using a closed system should additionally elucidate key biochemical signals and interactions taking place between hiPSC-EC and hiPSC-RPE in both healthy and simulated disease conditions.

Declaration of Competing Interest

The authors declare that they have no known competing financial interests or personal relationships that could have appeared to influence the work reported in this paper.

CRediT authorship contribution statement

Maria Teresa Calejo: Data curation, Formal analysis, Writing - original draft, Writing - review & editing, Validation. **Jaakko Saari:** Data curation, Formal analysis, Writing - original draft, Writing - review & editing, Validation. **Hanna Vuorenpää:** Writing - review & editing, Validation. **Elina Vuorimaa-Laukkanen:** Writing - review & editing, Validation. **Pasi Kallio:** Writing - review & editing, Validation, Funding acquisition. **Katriina Aalto-Setälä:** Writing - review & editing, Validation, Funding acquisition. **Susanna Miettinen:** Writing - review & editing, Validation, Funding acquisition. **Heli Skottman:** Writing - review & editing, Validation, Funding acquisition. **Minna Kellomäki:** Writing - review & editing, Validation, Funding acquisition. **Kati Juuti-Uusitalo:** Data curation, Formal analysis, Writing - original draft, Writing - review & editing, Validation, Funding acquisition.

Acknowledgments

Outi Melin, Hanna Pekkanen and Paula Puistola, are thanked for skilful technical assistance. The Zeiss LSM780 confocal microscope maintained by Tampere University imaging core was used in imaging. This work was supported by the Finnish Diabetes Foundation (KJ-U), the Eye and Tissue Bank Foundation (KJ-U), Evald and Hilda Nissi Foundation (KJ-U), the Academy of Finland (Centre of Excellence Body-on-Chip, MKe), the Competitive State Research Financing of the Expert Responsibility area of Tampere University Hospital (SMi), Business Finland (HSk, KA-S, PKa, MKe, SMi). The funders had no role in study design, data collection and analysis, decision to publish, or in the preparation of the manuscript.

Supplementary materials

Supplementary material associated with this article can be found, in the online version, at doi:10.1016/j.actbio.2019.11.002.

References

[1] J.M. Colijn, G.H.S. Buitendijk, E. Prokofyeva, D. Alves, M.L. Cachulo, A.P. Khawaja, A. Cougnard-Gregoire, B.M.J. Merle, C. Korb, M.G. Erke, A. Bron, E. Anastasopoulos, M.A. Meester-Smoor, T. Segato, S. Piermarocchi, P.T.V.M. de Jong, J.R. Vingerling, F. Topouzis, C. Creuzot-Garcher, G. Bertelsen, N. Pfeiffer, A.E. Fletcher, P.J. Foster, R. Silva, J.-F. Korobelnik, C. Delcourt, C.C.W. Klaver, S. Ajana, B. Arango-Gonzalez, V. Arndt, V. Bhatia, S.S. Bhattacharya, M. Biarnés, A. Borrell, S. Bühren, S.M. Calado, J.M. Colijn, A. Cougnard-Grégoire, S. Dammeier, E.K. de Jong, B. De la Cerda, C. Delcourt, A.I. den Hollander, F.J. Diaz-Corrales, S. Diether, E. Emri, T. Endermann, L.L. Ferraro, M. Garcia, T.J. Heesterbeek, S. Honisch, C.B. Hoyng, E. Kersten, E. Kilger, C.C.W. Klaver, H. Langen, I. Lengyel, P. Luthert, C. Maugeais, M. Meester-Smoor, B.M.J. Merle, J. Monés, E. Nogoceke, T. Peto, F.M. Pool, E. Rodríguez, M. Ueffing, K.U. Ulrich Bartz-Schmidt, E.M. van Leeuwen, T. Verzijden, M. Zumbansen, N. Acar, E. Anastosopoulos, A. Azuara-Blanco, A. Bergen, G. Bertelsen, C. Binquet, A. Bird, L. Brétillon, A. Bron, G. Buitendijk, M.L. Cachulo, U. Chakravarthy, M. Chan, P. Chang, J. Colijn, A. Cougnard-Grégoire, C. Creuzot-Garcher, P. Cumberland, J. Cunha-Vaz, V. Daien, G. Deak, C. Delcourt, M.-N. Delyfer, A. den Hollander, M. Dietzel, M.G. Erke, S. Fauser, R. Finger, A. Fletcher, P. Foster, P. Founti, A. Göbel, T. Gorgels, J. Grauslund, F. Grus, C. Hammond, C. Helmer, H.-W. Hense, M. Hermann, R. Hoehn, R. Hogg, F. Holz, C. Hoyng, N. Jansonius, S. Janssen, A. Khawaja, C. Klaver, J.-F. Korobelnik, J. Lamparter, M. Le Goff, S. Leal, Y. Lechanteur, T. Lehtimäki, A. Lotery, I. Leung, M. Mauschitz, B. Merle, V. Meyer zu Westrup, E. Midena, S. Miotto, A. Mirshahi, S. Mohan-Saïd, M. Mueller, A. Muldrew, S. Nunes, K. Oexle, T. Peto, S. Piermarocchi, E. Prokofyeva, J. Rahi, O. Raitakari, L. Ribeiro, M.-B. Rougier, J. Sahel, A. Salonikiou, C. Sanchez, S. Schmitz-Valckenberg, C. Schweitzer, T. Segato, J. Shehata, R. Silva, G. Silvestri, C. Simader, E. Souied, H. Springelkamp, R. Tapp, F. Topouzis, V. Verhoeven, T. Von Hanno, S. Vujosevic, K. Williams, C. Wolfram, J. Yip, J. Zerbib, I. Zwiener, Prevalence of age-related macular degeneration in Europe: the past and the future, Ophthalmology 124 (2017) 1753–1763.

[2] A. Biesemeier, T. Taubitz, S. Julien, E. Yoeruek, U. Schraermeyer, Choriocapillaris breakdown precedes retinal degeneration in age-related macular degeneration, Neurobiol. Aging. 35 (2014) 2562–2573.

[3] P.L. Müller, M. Pfau, P.T. Möller, J. Nadal, M. Schmid, M. Lindner, L. de Sisternes, H. Stöhr, B.H.F. Weber, C. Neuhaus, P. Herrmann, S. Schmitz-Valckenberg, F.G. Holz, M. Fleckenstein, Choroidal flow signal in late-onset Stargardt disease and age-related macular degeneration: an OCT-angiography study, Invest. Ophthalmol. Vis. Sci. 59 (2018) AMD122–AMD131.

[4] J.C. Booij, D.C. Baas, J. Beisekeeva, T.G.M.F. Gorgels, A.A.B. Bergen, The dynamic nature of Bruch's membrane, Prog Retin Eye Res 29 (2010) 1–18.

[5] T.-C. Lin, M.J. Seiler, D. Zhu, P. Falabella, D.R. Hinton, D.O. Clegg, M.S. Humayun, B.B. Thomas, Assessment of safety and functional efficacy of stem cell-based therapeutic approaches using retinal degenerative animal models, Stem Cells Int. 19 (2017) 9428176.

[6] S. Shafaie, V. Hutter, M.T. Cook, M.B. Brown, D.Y.S. Chau, *In vitro* cell models for ophthalmic drug development applications, Biores Open Access 5 (2016) 94–108.

[7] J. Adijanto, N.J. Philp, Cultured primary human fetal retinal pigment epithelium (hfRPE) as a model for evaluating RPE metabolism, Exp. Eye Res. 126 (2014) 77–84.

[8] W. Fan, J.J. Zheng, B.J. McLaughlin, An *in vitro* model of the back of the eye for studying retinal pigment epithelial-choroidal endothelial interactions, In Vitro Cell.Dev.Biol. Animal. 38 (2002) 228–234.

[9] G.E. Korte, V. Reppucci, P. Henkind, RPE destruction causes choriocapillary atrophy, Invest. Ophthalmol. Vis. Sci. 25 (1984) 1135–1145.

[10] H.G.T. Blaauwgeers, G.M. Holtkamp, H. Rutten, A.N. Witmer, P. Koolwijk, T.A. Partanen, K. Alitalo, M.E. Kroon, A. Kijlstra, V.W.M. van Hinsbergh, R.O. Schlingemann, Polarized vascular endothelial growth factor secretion by human retinal pigment epithelium and localization of vascular endothelial growth factor receptors on the inner choriocapillaris, Am. J. Pathol. 155 (1999) 421–428.

[11] R. Dardik, T. Livnat, G. Halpert, S. Jawad, Y. Nisgav, S. Azar-Avivi, B. Liu, R.B. Nussenblatt, D. Weinberger, B. Sredni, The small tellurium-based compound SAS suppresses inflammation in human retinal pigment epithelium, Mol. Vis. 22 (2016) 548–562.

[12] P. Geisen, J.R. McColm, M. Elizabeth Hartnett, Choroidal endothelial cells transmigrate across the retinal pigment epithelium but do not proliferate in response to soluble vascular endothelial growth factor, Exp. Eye Res. 82 (2006) 608–619.

[13] H. Wang, P. Geisen, E.S. Wittchen, B. King, K. Burridge, P.A. D'Amore, M.E. Hartnett, The role of RPE cell-associated VEGF189 in choroidal endothelial cell transmigration across the RPE, Invest. Ophthalmol. Vis. Sci. 52 (2011) 570–578.

[14] C. Spencer, S. Abend, K.J. McHugh, M. Saint-Geniez, Identification of a synergistic interaction between endothelial cells and retinal pigment epithelium, J. Cell. Mol. Med. 21 (2017) 2542–2552.

[15] T. Sakamoto, H. Sakamoto, T.L. Murphy, C. Spee, D. Soriano, T. Ishibashi, D.R. Hinton, S.J. Ryan, Vessel formation by choroidal endothelial cells *in vitro* is modulated by retinal pigment epithelial cells, Arch. Ophthalmol. 113 (1995) 512–520.
[16] R.D. Hamilton, A.J. Foss, L. Leach, Establishment of a human *in vitro* model of the outer blood-retinal barrier, J Anat 211 (2007) 707–716.
[17] S. Chen, S. Gao, J. Jing, Q. Lu, Designing 3D biological surfaces via the breath–figure method, Adv. Healthc. Mater. 7 (2018) 1701043.
[18] M.T. Calejo, T. Ilmarinen, H. Skottman, M. Kellomäki, Breath figures in tissue engineering and drug delivery: state-of-the-art and future perspectives, Acta Biomater. 66 (2018) 44–66.
[19] M.T. Calejo, T. Ilmarinen, E. Vuorimaa-Laukkanen, E. Talvitie, H.M. Hakola, H. Skottman, M. Kellomäki, Langmuir–Schaefer film deposition onto honeycomb porous films for retinal tissue engineering, Acta Biomater. 54 (2017) 138–149.
[20] M.T. Calejo, T. Ilmarinen, H. Jongprasitkul, H. Skottman, M. Kellomäki, Honeycomb porous films as permeable scaffold materials for human embryonic stem cell-derived retinal pigment epithelium, Biomed. Mater. Res. 104 (2016) 1646–1656.
[21] M.T. Calejo, A. Haapala, H. Skottman, M. Kellomäki, Porous polybutylene succinate films enabling adhesion of human embryonic stem cell-derived retinal pigment epithelial cells (hESC-RPE), Eur. Polym. J. 118 (2019) 78–87.
[22] K. Ariga, Y. Yamauchi, T. Mori, J.P. Hill, 25th anniversary article: what can be done with the Langmuir–Blodgett method? Recent developments and its critical role in materials science, Adv. Mater. 25 (2013) 6477–6512.
[23] K. Blodgett, Monomolecular films of fatty acids on glass, J. Am. Chem. Soc. 56 (1934) 495 –495.
[24] D.M. Rabin, R.L. Rabin, T.A. Blenkinsop, S. Temple, J.H. Stern, Chronic oxidative stress upregulates Drusen-related protein expression in adult human RPE stem cell-derived RPE cells: a novel culture model for dry AMD, Aging (Albany NY) 5 (2012) 51–66.
[25] J. Tian, K. Ishibashi, J.T. Handa, The expression of native and cultured RPE grown on different matrices, Physiol. Genomics 17 (2004) 170–182.
[26] N.V. Strunnikova, A. Maminishkis, J.J. Barb, F. Wang, C. Zhi, Y. Sergeev, W. Chen, A.O. Edwards, D. Stambolian, G. Abecasis, A. Swaroop, P.J. Munson, S.S. Miller, Transcriptome analysis and molecular signature of human retinal pigment epithelium, Hum. Mol. Genet. 19 (2010) 2468–2486.
[27] I. Klimanskaya, J. Hipp, K.A. Rezai, M. West, A. Atala, R. Lanza, Derivation and comparative assessment of retinal pigment epithelium from human embryonic stem cells using transcriptomics, Cloning Stem Cells 6 (2004) 217–245.
[28] H. Vaajasaari, T. Ilmarinen, K. Juuti-Uusitalo, K. Rajala, N. Onnela, S. Narkilahti, R. Suuronen, J. Hyttinen, H. Uusitalo, H. Skottman, Toward the defined and xeno-free differentiation of functional human pluripotent stem cell-derived retinal pigment epithelial cells, Mol. Vis. 17 (2011) 558–575.
[29] Y. Hirami, F. Osakada, K. Takahashi, K. Okita, S. Yamanaka, H. Ikeda, N. Yoshimura, M. Takahashi, Generation of retinal cells from mouse and human induced pluripotent stem cells, Neurosci. Lett. 458 (2009) 126–131.
[30] D.E. Buchholz, S.T. Hikita, T.J. Rowland, A.M. Friedrich, C.R. Hinman, L.V. Johnson, D.O. Clegg, Derivation of functional retinal pigmented epithelium from induced pluripotent stem cells, Stem Cells 27 (2009) 2427–2434.
[31] D.E. Buchholz, B.O. Pennington, R.H. Croze, C.R. Hinman, P.J. Coffey, D.O. Clegg, Rapid and efficient directed differentiation of human pluripotent stem cells into retinal pigmented epithelium, Stem Cells Transl. Med. 2 (2013) 384–393.
[32] J.S. Meyer, S.E. Howden, K.A. Wallace, A.D. Verhoeven, L.S. Wright, E.E. Capowski, I. Pinilla, J.M. Martin, S. Tian, R. Stewart, B. Pattnaik, J.A. Thomson, D.M. Gamm, Optic vesicle-like structures derived from human pluripotent stem cells facilitate a customized approach to retinal disease treatment, Stem Cells 29 (2011) 1206–1218.
[33] B.B. Thomas, D. Zhu, L. Zhang, P.B. Thomas, Y. Hu, H. Nazari, F. Stefanini, P. Falabella, D.O. Clegg, D.R. Hinton, M.S. Humayun, Survival and functionality of hESC-derived retinal pigment epithelium cells cultured as a monolayer on polymer substrates transplanted in rcs rats, Invest. Ophthalmol. Vis. Sci. 57 (2016) 2877–2887.
[34] A. Subrizi, H. Hiidenmaa, T. Ilmarinen, S. Nymark, P. Dubruel, H. Uusitalo, M. Yliperttula, A. Urtti, H. Skottman, Generation of hESC-derived retinal pigment epithelium on biopolymer coated polyimide membranes, Biomaterials 33 (2012) 8047–8054.
[35] A.E. Sorkio, E.P. Vuorimaa-Laukkanen, H.M. Hakola, H. Liang, T.A. Ujula, J.J. Valle-Delgado, M. Österberg, M.L. Yliperttula, H. Skottman, Biomimetic collagen I and IV double layer Langmuir–Schaefer films as microenvironment for human pluripotent stem cell derived retinal pigment epithelial cells, Biomaterials 51 (2015) 257–269.
[36] A. Sorkio, P.J. Porter, K. Juuti-Uusitalo, B.J. Meenan, H. Skottman, G.A. Burke, Surface modified biodegradable electrospun membranes as a carrier for human embryonic stem cell-derived retinal pigment epithelial cells, Tissue Eng. Part A (2015).
[37] T. Ilmarinen, H. Hiidenmaa, P. Kööbi, S. Nymark, A. Sorkio, J.-H. Wang, B.V. Stanzel, F. Thieltges, P. Alajuuma, O. Oksala, M. Kataja, H. Uusitalo, H. Skottman, Ultrathin polyimide membrane as cell carrier for subretinal transplantation of human embryonic stem cell derived retinal pigment epithelium, PLoS ONE (2015) 10.
[38] A. Sorkio, S. Haimi, V. Verdoold, K. Juuti-Uusitalo, D. Grijpma, H. Skottman, Poly(trimethylene carbonate) as an elastic biodegradable film for human embryonic stem cell-derived retinal pigment epithelial cells, J. Tissue Eng. Regen. Med. 11 (2017) 3134–3144.
[39] M.P. White, A.J. Rufaihah, L. Liu, Y.T. Ghebremariam, K.N. Ivey, J.P. Cooke, D. Srivastava, Limited gene expression variation in human embryonic stem cell and induced pluripotent stem cell-derived endothelial cells, Stem Cells 31 (2013) 92–103.
[40] R. Samuel, L. Daheron, S. Liao, T. Vardam, W.S. Kamoun, A. Batista, C. Buecker, R. Schäfer, X. Han, P. Au, D.T. Scadden, D.G. Duda, D. Fukumura, R.K. Jain, Generation of functionally competent and durable engineered blood vessels from human induced pluripotent stem cells, PNAS 110 (2013) 12774–12779.
[41] V.V. Orlova, F.E. van den Hil, S. Petrus-Reurer, Y. Drabsch, P. ten Dijke, C.L. Mummery, Generation, expansion and functional analysis of endothelial cells and pericytes derived from human pluripotent stem cells, Nat. Protoc. 9 (2014) 1514–1531.
[42] S. Rosa, C. Praça, P.R. Pitrez, P.J. Gouveia, X.L. Aranguren, L. Ricotti, L.S. Ferreira, Functional characterization of iPSC-derived arterial- and venous-like endothelial cells, Sci. Rep. 9 (2019).
[43] M. Ojala, C. Prajapati, R.-P. Pölönen, K. Rajala, M. Pekkanen-Mattila, J. Rasku, K. Larsson, K. Aalto-Setälä, Mutation-specific phenotypes in hiPSC-derived cardiomyocytes carrying either myosin-binding protein *c* or α-tropomyosin mutation for hypertrophic cardiomyopathy, Stem Cells Int. 2016 (2016) 1684792.
[44] H. Hongisto, T. Ilmarinen, M. Vattulainen, A. Mikhailova, H. Skottman, Xeno- and feeder-free differentiation of human pluripotent stem cells to two distinct ocular epithelial cell types using simple modifications of one method, Stem Cell Res. Ther. 8 (2017) 291.
[45] X. Liu, J. Qi, X. Xu, M. Zeisberg, K. Guan, E.M. Zeisberg, Differentiation of functional endothelial cells from human induced pluripotent stem cells: a novel, highly efficient and cost effective method, Differentiation 92 (2016) 225–236.
[46] J.-R. Sarkanen, H. Vuorenpää, O. Huttala, B. Mannerström, H. Kuokkanen, S. Miettinen, T. Heinonen, T. Ylikomi, Adipose stromal cell tubule network model provides a versatile tool for vascular research and tissue engineering, Cells Tissues Organs (Print) 196 (2012) 385–397.
[47] O. Huttala, H. Vuorenpää, T. Toimela, J. Uotila, H. Kuokkanen, T. Ylikomi, J.-R. Sarkanen, T. Heinonen, Human vascular model with defined stimulation medium - a characterization study, ALTEX 32 (2015) 125–136.
[48] F. Verseijden, H. Jahr, S.S. Posthumus-van, T.H. Ten, S.E. Hovius, A.L. Seynhaeve, J.N. Van, G.O. Van, S.O. Hofer, Angiogenic capacity of human adipose-derived stromal cells during adipogenic differentiation: an *in vitro* study, Tissue Eng. Part A 15 (2009) 445–452.
[49] T. Ikuno, H. Masumoto, K. Yamamizu, M. Yoshioka, K. Minakata, T. Ikeda, R. Sakata, J.K. Yamashita, Efficient and robust differentiation of endothelial cells from human induced pluripotent stem cells via lineage control with VEGF and cyclic AMP, PLoS ONE 12 (2017) e0173271.
[50] T. Nishikawa, R. Ookura, J. Nishida, K. Arai, J. Hayashi, N. Kurono, T. Sawadaishi, M. Hara, M. Shimomura, Fabrication of honeycomb film of an amphiphilic copolymer at the air−water interface, Langmuir 18 (2002) 5734–5740.
[51] L.-S. Wan, J.-W. Li, B.-B. Ke, Z.-K. Xu, Ordered microporous membranes templated by breath figures for size-selective separation, J. Am. Chem. Soc. 134 (2012) 95–98.
[52] Y. Fukuhira, H. Yabu, K. Ijiro, M. Shimomura, Interfacial tension governs the formation of self-organized honeycomb-patterned polymer films, Soft Matter. 5 (2009) 2037–2041.
[53] Y. Yuan, T.R. Lee, Contact angle and wetting properties, in: Surface Science Techniques, Springer, Berlin, Heidelberg, 2013, pp. 3–34.
[54] D. Öner, T.J. McCarthy, Ultrahydrophobic surfaces. effects of topography length scales on wettability, Langmuir 16 (2000) 7777–7782.
[55] Z. Li, X. Ma, Q. Kong, D. Zang, X. Guan, X. Ren, Static and dynamic hydrophobic properties of honeycomb structured films via breath figure method, J. Phys. Chem. C 120 (2016) 18659–18664.
[56] A.A. Hussain, C. Starita, A. Hodgetts, J. Marshall, Macromolecular diffusion characteristics of ageing human Bruch's membrane: implications for age-related macular degeneration (AMD), Exp. Eye Res. 90 (2010) 703–710.
[57] H.-J. Sung, C. Meredith, C. Johnson, Z.S. Galis, The effect of scaffold degradation rate on three-dimensional cell growth and angiogenesis, Biomaterials 25 (2004) 5735–5742.
[58] R.M. Leblanc, Q. Huo, Langmuir and langmuir-blodgett films of proteins and enzymes, in: Encyclopedia of Surface and Colloid Science, third ed., CRC Press, 2015, pp. 3545–3571.
[59] A.J.J. Goffin, J. Rajadas, G.G. Fuller, Interfacial flow processing of collagen, Langmuir 26 (2010) 3514–3521.
[60] J.M. Roberts, J.V. Forrester, Factors affecting the migration and growth of endothelial cells from microvessels of bovine retina, Exp. Eye Res. 50 (1990) 165–172.
[61] M. Bahramsoltani, I. Slosarek, W.D. Spiegelaere, J. Plendl, Angiogenesis and collagen type IV expression in different endothelial cell culture systems, Anat Histol Embryol 43 (2014) 103–115.
[62] O.V. Halaidych, C. Freund, F. van den Hil, D.C.F. Salvatori, M. Riminucci, C.L. Mummery, V.V. Orlova, Inflammatory responses and barrier function of endothelial cells derived from human induced pluripotent stem cells, Stem Cell Rep. 10 (2018) 1642–1656.
[63] P. Simara, L. Tesarova, D. Rehakova, S. Farkas, B. Salingova, K. Kutalkova, E. Vavreckova, P. Matula, P. Matula, L. Veverkova, I. Koutna, Reprogramming of adult peripheral blood cells into human induced pluripotent stem cells as a safe and accessible source of endothelial cells, Stem Cells Dev. 27 (2018) 10–22.

[64] R. Olmer, L. Engels, A. Usman, S. Menke, M.N.H. Malik, F. Pessler, G. Göhring, D. Bornhorst, S. Bolten, S. Abdelilah-Seyfried, T. Scheper, H. Kempf, R. Zweigerdt, U. Martin, Differentiation of human pluripotent stem cells into functional endothelial cells in scalable suspension culture, Stem Cell Rep. 10 (2018) 1657–1672.
[65] K. Arai, M. Tanaka, S. Yamamoto, M. Shimomura, Effect of pore size of honeycomb films on the morphology, adhesion and cytoskeletal organization of cardiac myocytes, Coll. Surf. A Physicochem. Eng. Aspects 313–314 (2008) 530–535.
[66] H. Sunami, E. Ito, M. Tanaka, S. Yamamoto, M. Shimomura, Effect of honeycomb film on protein adsorption, cell adhesion and proliferation, Coll. Surf. A Physicochem. Eng. Aspects 284–285 (2006) 548–551.
[67] X. Wu, S. Wang, Regulating MC3T3-E1 cells on deformable poly(ε-caprolactone) honeycomb films prepared using a surfactant-free breath figure method in a water-miscible solvent, ACS Appl. Mater. Interfaces. 4 (2012) 4966–4975.
[68] M.A. Birch, M. Tanaka, G. Kirmizidis, S. Yamamoto, M. Shimomura, Microporous "honeycomb" films support enhanced bone formation *in vitro*, Tissue Eng. Part A 19 (2013) 2087–2096.
[69] J.R. McMillan, M. Akiyama, M. Tanaka, S. Yamamoto, M. Goto, R. Abe, D. Sawamura, M. Shimomura, H. Shimizu, Small-diameter porous poly (ε-caprolactone) films enhance adhesion and growth of human cultured epidermal keratinocyte and dermal fibroblast cells, Tissue Eng. 13 (2007) 789–798.
[70] T. Nishikawa, M. Nonomura, K. Arai, J. Hayashi, T. Sawadaishi, Y. Nishiura, M. Hara, M. Shimomura, Micropatterns based on deformation of a viscoelastic honeycomb mesh, Langmuir 19 (2003) 6193–6201.
[71] T. Nishikawa, K. Arai, J. Hayashi, M. Hara, M. Shimomura, Honeycomb films": biointerface for tissue engineering, Int. J. Nanosci. 01 (2002) 415–418.
[72] J.B. Jonas, L. Holbach, S. Panda-Jonas, Bruch's membrane thickness in high myopia, Acta Ophthalmol. (Copenh.) 92 (2014) e470–e474.
[73] H. Skottman, J. Muranen, H. Lähdekorpi, E. Pajula, K. Mäkelä, L. Koivusalo, A. Koistinen, H. Uusitalo, K. Kaarniranta, K. Juuti-Uusitalo, Contacting co-culture of human retinal microvascular endothelial cells alters barrier function of human embryonic stem cell derived retinal pigment epithelial cells, Exp. Cell Res. 359 (2017) 101–111.
[74] I. Benedicto, G.L. Lehmann, M. Ginsberg, D.J. Nolan, R. Bareja, O. Elemento, Z. Salfati, N.M. Alam, G.T. Prusky, P. Llanos, S.Y. Rabbany, A. Maminishkis, S.S. Miller, S. Rafii, E. Rodriguez-Boulan, Concerted regulation of retinal pigment epithelium basement membrane and barrier function by angiocrine factors, Nat Commun. 8 (2017) 15374.
[75] J. Wisniewska-Kruk, K.A. Hoeben, I.M.C. Vogels, P.J. Gaillard, C.J.F. Van Noorden, R.O. Schlingemann, I. Klaassen, A novel co-culture model of the blood-retinal barrier based on primary retinal endothelial cells, pericytes and astrocytes, Exp. Eye Res. 96 (2012) 181–190.
[76] Y. Iwata, W.D. Klaren, C.S. Lebakken, F.A. Grimm, I. Rusyn, High-content assay multiplexing for vascular toxicity screening in induced pluripotent stem cell-derived endothelial cells and human umbilical vein endothelial cells, Assay Drug. Dev. Technol. 15 (2017) 267–279.
[77] M. Tanaka, A. Takayama, E. Ito, H. Sunami, S. Yamamoto, M. Shimomura, Effect of pore size of self-organized honeycomb-patterned polymer films on spreading, focal adhesion, proliferation, and function of endothelial cells, J. Nanosci. Nanotechnol. 7 (2007) 763–772.
[78] P.A. Campochiaro, Retinal and choroidal neovascularization, J. Cell. Physiol 184 (2000) 301–310.
[79] M.E. Hartnett, A. Lappas, D. Darland, J.R. McColm, S. Lovejoy, P.A. D'Amore, Retinal pigment epithelium and endothelial cell interaction causes retinal pigment epithelial barrier dysfunction via a soluble VEGF-dependent mechanism, Exp. Eye Res. 77 (2003) 593–599.
[80] V.V. Orlova, Y. Drabsch, C. Freund, S. Petrus-Reurer, F.E. van den Hil, S. Muenthaisong, P.T. Dijke, C.L. Mummery, Functionality of endothelial cells and pericytes from human pluripotent stem cells demonstrated in cultured vascular plexus and zebrafish xenografts, Arterioscler. Thromb. Vasc. Biol. 34 (2014) 177–186.
[81] A.J. Rufaihah, N.F. Huang, J. Kim, J. Herold, K.S. Volz, T.S. Park, J.C. Lee, E.T. Zambidis, R. Reijo-Pera, J.P. Cooke, Human induced pluripotent stem cell-derived endothelial cells exhibit functional heterogeneity, Am. J. Transl. Res. 5 (2013) 21–35.
[82] H. Vazão, S. Rosa, T. Barata, R. Costa, P.R. Pitrez, I. Honório, M.R. de Vries, D. Papatsenko, R. Benedito, D. Saris, A. Khademhosseini, P.H.A. Quax, C.F. Pereira, N. Mercader, H. Fernandes, L. Ferreira, High-throughput identification of small molecules that affect human embryonic vascular development, PNAS 114 (2017) E3022–E3031.